Title

+3 THE ABSORPTION SPECTRUM OP Cf AND CRYSTALLOGRAPHY OF CALIFORNIUM SESQUIOXIDE AND CALIFORNIUM TRICHLORIDE

Author

Green, J.L.

Publication Date

1965-11-01

UCRL-16516

University of California

Ernest O. Lawrence Radiation Laboratory

THE ABSORPTION SPECTRUM OF Cf^{+3} AND CRYSTALLOGRAPHY OF CALIFORNIUM SESQUIOXIDE AND CALIFORNIUM TRICHLORIDE

Berkeley, California

DISCLAIMER

Research and Development

UCRL-16516

UNIVERSITY OF CALIFORNIA

Lawrence Radiation Laboratory
Berkeley, California

AEC Contract No. W-7405-eng-48

THE ABSORPTION SPECTRUM OF Cf^{+3} AND CRYSTALLOGRAPHY OF CALIFORNIUM SESQUIOXIDE AND CALIFORNIUM TRICHLORIDE

J. L. Green
(Ph.D. Thesis)

November 1965

THE ABSORPTION SPECTRUM OF Cf^{+3} AND CRYSTALLOGRAPHY OF CALIFORNIUM SESQUIOXIDE AND CALIFORNIUM TRICHLORIDE

Contents

Abstract v

I. Introduction 1

II. Purification and Analytical Work 3

A. Sources of Cf^{249} 6

B. Reagents 7

1. Initial Operations 7

2. High Purity Operations 7

C. Ion Exchange Column Operation 11

D. Purification Operation Flowsheets 15

E. Analytical Techniques 15

1. Mass Analysis for Neodymium 18

2. Actinide Analyses 20

3. Emission Spectroscopic Analysis 24

4. Single Ion Exchange Bead Assays 26

III. Absorption Spectra of Cf^{+3} 32

A. Spectrum of Californium Absorbed on Cation Exchange Beads 32

B. Spectrum of Hydrated Californium Trichloride 38

C. Absorption Spectrum of Californium in a Single Crystal of Anhydrous $CfCl_3$ 41

IV. Compound Preparation and Crystallographic Studies 57

A. Compound Preparations 57

1. Bead Ignition 57

2. Californium Sesquioxide 60

3. Californium Trichloride 62

B. Crystallographic Investigations 63

1. Californium Sesquioxide 66

2. Californium Trichloride 75

V. Summary 86

Acknowledgments 88

References 89

THE ABSORPTION SPECTRUM OF Cf^{+3} AND CRYSTALLOGRAPHY OF CALIFORNIUM SESQUIOXIDE AND CALIFORNIUM TRICHLORIDE

J. L. Green

Lawrence Radiation Laboratory
University of California
Berkeley, California

November 1965

ABSTRACT

The work reported here was undertaken for the purpose of extending existing knowledge of the chemical and physical properties of element 98, californium. An essential preliminary to these studies was the development of satisfactory techniques for obtaining microgram amounts of the element in a state of satisfactory chemical purity, and for utilizing this material in spectroscopic and crystallographic investigations.

The general problems involved in small scale purification operations are discussed. The procedures used for the purification of approximately 6 μg of Cf^{249} are described in detail as are the analytical techniques used for purity evaluations. Adequate purity with respect to lanthanides and other actinides was demonstrated with reasonable certainty; however, it is shown that other materials are potentially present as contaminants. Arguments are presented which justify the postulation that these materials are probably Ca and/or Al.

A detailed discussion is given of the techniques which were developed for obtaining the absorption spectrum of microsamples of Cf^{+3}. Absorption spectrum data from 400 mμ to 800 mμ are presented for Cf^{+3} absorbed in cation exchange resin beads and for solid hydrated californium trichloride. The spectrum of these materials is expected to be very similar to the spectrum of Cf^{+3} in solution. A sample of anhydrous $CfCl_3$ was prepared that apparently is a single crystal. Room temperature absorption spectra from 4000 A to 9000 A were taken of this

material. Tentative calculations are presented which fit these data to a theoretical energy level scheme.

Several polycrystalline samples of californium sesquioxide were prepared and studied using x-ray diffraction techniques. The structure exhibited by these samples was the monoclinic Sm_2O_3 structure having $a = 14.124 \pm 0.020$ A, $b = 3.591 \pm 0.003$ A, $c = 8.809 \pm 0.013$ A and $\beta = 100.31 \pm 0.02$ deg. Similarly, preparations of $CfCl_3$ were found to exhibit the hexagonal UCl_3 structure having $a = 7.393 \pm 0.040$ A and $c = 4.090 \pm 0.060$ A. The ionic radius for californium computed from the trichloride data is 0.98 A. The error limits reported here are based on a statistical evaluation of the consistency of a group of determinations, accounting for nonstatistical sampling, and do not reflect the internal consistency of the data from the individual preparations.

I. INTRODUCTION

The recent increase in the availability of the heavy man-made actinides[1] has made it possible to begin to study the bulk chemical and physical properties of these elements and their compounds. The notable work of B. B. Cunningham and J. C. Wallmann on the single ion exchange bead technique[2,3] has made these investigations possible when only submicrogram amounts of pure material are available. The procedure these workers devised begins with the absorption of the isotope of interest on a single bead of cation exchange resin. When saturated, these beads constitute a highly concentrated sample, bound in a mechanically coherent particle which may be relatively easily manipulated without loss of activity. The material may be removed from the organic sulfonate matrix without destroying the particulate nature of the sample by high temperature air ignition of the bead. This produces a single, coherent, spherical particle of the air stable oxide of the element. From this point, the preparation of a wide variety of compounds is possible through the application of appropriate anhydrous preparative procedures.

In this study these techniques were refined to insure better chemical purity of the material of interest and were broadened to embrace moderate and high-dispersion room temperature absorption spectroscopy of submicrogram samples. A problem of grave concern when very small amounts of material are involved is that of sample purity. Only relatively recently has the magnitude of the sensitivity of these systems to contamination been fully recognized. This difficulty has been of particular interest during this study and, although no final solution has been discovered, significant advances in purification technique and purity evaluation have been made.

In the systematic exploration of the chemistry of californium, the determination of the absorption spectrum of the tripositive ion seems to be a logical early objective. The spectrum of the aqueous ion

would serve as a convenient means of analysis and identification in future studies. Although the solution spectrum of californium was not directly observed in this study, the spectrum of the ion absorbed on ion exchange resin was recorded. Based on the observation that the spectra of Pr, Nd and Pu absorbed on cation resin are essentially the same as the solution spectra, it is suggested that a similar correspondence exists in the case of californium. In addition, the spectrum of Cf^{+3} in a crystal of anhydrous $CfCl_3$ was recorded. Such data provides an experimental basis for the evaluation of the various spectroscopic parameters which have been applied to the interpretation of the spectra of the lanthanides and lighter actinides.

The availability of techniques applicable to the preparation of pure solid compounds makes possible crystallographic studies which serve to characterize the behavior of californium in solid crystalline systems. Preliminary studies of this nature have been carried out on californium sesquioxide and californium trichloride.

II. PURIFICATION AND ANALYTICAL WORK

One of the major obstacles to the investigation of the chemical behavior of the heavy actinides is the difficulty of preparing samples of the materials of interest in a state of adequate purity. The difficulties that arise are due, in large part, to the scale of the purification operations. Often, a quantity ranging from a few hundred nanograms to a few micrograms of the isotope of interest is all that is available for study. Even using microtechniques, purifying this small an amount of an isotope with high atomic weight involves the handling of very dilute solutions. Working with these materials at low concentration makes the system hypersensitive to recontamination, particularly with respect to impurities having low atomic weights.

For the purpose of this discussion, it is advantageous to separate the sources of cationic contaminants into two general categories, i.e., primary sources and background sources. Primary sources are those which are of concern in any purification procedure, regardless of scale. This group consists principally of those contaminants initially present in the unpurified material. It should be possible, using standard techniques, to efficiently remove all impurities introduced from primary origins.

Background sources, on the other hand, are those responsible for unintentional recontamination during and after purification. The relative importance of this category depends to a large extent on the scale of the operation. In large scale processing, where the concentration of the material of interest is relatively high, these sources are ordinarily of minor importance. When, however, very small amounts of material are involved, they can become highly significant. A few of the more important sources of this type are listed as follows:

1. Reagents. In a practical sense, it is impossible to prepare reagents that are absolutely pure, i.e., some level of background contamination is always present. In order for a reagent to be acceptable for use in a purification operation, it is necessary that the

amounts of the contaminants be sufficiently small with respect to the amount of the product material during processing. When dealing with dilute solutions of materials with high atomic weights, the requirements for reagent purity become quite stringent. Table I illustrates the general magnitude of the sensitivity of final product purity to the atomic weight of the contaminant and to the total solution volume encountered by the product after the last quantitative separation from a particular impurity.

2. Surfaces. The interaction of reagents with the surfaces of containment vessels has been found to be an important source of contaminants in micropurification work. It is essential that high purity operations be carried out in vessels that have been carefully cleaned to remove impurities on and in the surfaces which contact the product solutions. It is further necessary to fabricate vessels of materials that are either impervious to attack by the solution or at least are attacked to a minor extent. This care must be exercised not only with containers but with any surface that contacts the solutions, i.e., pipettes, ion exchange columns, etc. The principal material used in this study for high purity operations was fused silica.

3. Dust. Airborne laboratory dust is a particularly serious problem in that it is difficult to estimate the amount or the kind of contaminants introduced from this source. The dust encountered is derived from several distinct sources, both external and internal to the laboratory; e.g., natural and synthetic fibers, largely organic but possibly containing biologically prominent cations; terrestrial dust containing a high proportion of Si, Ca, Al, and Mg; industrial dust which often contains considerable amounts of iron and aluminum oxides; and finally, laboratory dust, which can be an especially serious source of undesirable contaminants. In the ordinary laboratory, one encounters large quantities of powdery inorganic compounds and relatively large amounts of metallic corrosion products which are easily transported by air currents. The only real defense against dust is the confinement

Table I. Concentration of contaminants in reagents to produce 0.1 atom % contamination of 5 μg of Cf^{249}.

Total processing volume after separation (λ)	(ng contaminant/ml reagent); (parts per billion)			
	Be	Al	Ca	Nd
10	18	54	80	290
50	4	11	16	58
100	2	5	8	29
500	0.4	1	2	6

of purification operations to dust free enclosures; however, if this is not feasible, caution is the only alternative.

Background contamination is, to a large extent, unpredictable and, therefore, difficult to control. The essential difference between primary and background contaminants is that it should be possible to remove primary impurities completely while background contaminants are always present to some extent. Virtually any real process will introduce some quantity of impurities. Since it is not possible to eliminate background impurities, the problem becomes one of confining their concentration to an acceptable level. This may be done by first minimizing the availability of contaminants, i.e., operating in very clean systems and using very pure reagents and second by maximizing the concentration of the material of interest by volumetrically scaling down the operations.

A. Sources of Cf^{249}

The preliminary investigations in this study were carried out using approximately 3 μg of Cf^{249} which had been derived from residues from earlier work. These residues were carefully chosen to eliminate any substantial amounts of Cf^{252} in an attempt to avoid the γ and neutron radiation associated with this isotope. At a later date an additional 3 μg was obtained by "milking" a Bk^{249} source which had previously been purified with respect to other actinides. The actinide purifications and californium "milking" operations were done using HDEHP (hydrogen di(2-ethylhexyl) orthophosphoric acid) extraction cycles.[4] Since the only concern with the isotopic composition of the material was associated with possible radiation problems, no isotopic analyses were performed.

B. Reagents

1. Initial Operations

For the initial purification operations, the reagents were prepared from stock C.P. chemicals. The only exceptions to this were water and α-hydroxyisobutyric acid, "but". The water was the once redistilled material derived from the continuous overflow from the two stage quartz still used for the preparation of high purity water. The "but" was purified by dissolution in pure water, filtration and partial recrystallization.

2. High Purity Operations

In the final purification operations, the only reagents required were water and various HCl solutions.

a. Water. The high purity quartz distilled water used in this work was supplied by Dr. Maynard Michel of this laboratory. The technique used for its preparation has been discussed elsewhere[5]; however, for completeness, the purification procedure will be briefly described here.

The starting material is ordinary distilled water. This is passed through a 1.5 inch diameter by 3 feet long mixed resin ion exchange column constructed completely of polytetrafluoroethylene (teflon). The effluent from the column is continuously introduced, via polypropylene tubing, into the first stage of a two stage continuous quartz still. Both stages operate with a continuous overflow to avoid the concentration of contaminants in the boilers. The overflow from the second stage is the source of the intermediate purity water (conductivity water) mentioned above. The condensate from the second stage is piped through polypropylene to a specially prepared polyethylene containers for storage. A typical spectrographic analysis of the product is shown in Table II. This particular batch of water was used in the preparation of the reagents for the high purity operations in the second purification cycle.

Table II. Spectroscopic analyses of high purity reagents used in the second purification cycle.[a]

	(ng/ml); (parts per billion)									
	Al	Be	Ca	Ce	Fe	K	La	Mg	Na	Si
Water	< 5	<0.1	20	-	<30	<3000	-	< 5	<3000	-
Saturated HCl	10	-	20	<50	<30	-	< 5	< 5	<3000	20
6 M HCl	20	<0.1	< 5	<50	<30	<3000	< 5	< 5	<3000	< 5
2 M HCl	< 5	<0.1	< 5	<50	<30	<3000	< 5	< 5	<3000	< 5
0.05 M HCl	< 5	<0.1	< 5	<50	<30	<3000	< 5	< 5	<3000	< 5
Alcoholic HCl	10	<0.1	< 5	<50	<30	<3000	< 5	< 5	<3000	< 5

[a]The limits of detection for this analysis are listed in Ref. 6.

b. HCl Solutions. Several techniques for the preparation of high purity HCl solutions were investigated; however, only one was studied thoroughly. This procedure was basically quite simple and has been shown to be adequate. Room-temperature-saturated HCl was prepared by the treatment of quartz distilled water, contained in a specially cleaned polyethylene bottle, with purified anhydrous HCl gas. A schematic diagram of the apparatus used is shown in Fig. 1. The source of HCl gas was preparative grade tank HCl which was allowed to flow slowly through a pyrex entrainment trap, a pyrex prebubbler containing saturated HCl solution, and finally through a second pyrex entrainment trap and a leached quartz-wool plug filter. All lines between the quartz-wool filter and the bubbler tube were made of leached quartz tubing. After the preparation and analysis of saturated HCl, other concentrations of aqueous HCl were made by dilution with high purity water in specially cleaned polyethylene containers. Room temperature saturated alcoholic HCl was prepared by making a 20 volume % solution of C.P. absolute ethanol in saturated aqueous HCl and resaturating at room temperature using the bubbler with alcoholic HCl in the prebubbler.

The polyethylene containers used for the preparation and storage of high purity reagents were prepared as follows:

1. Rinse thoroughly with distilled water.
2. Leach several days with C.P. concentrated HCl.
3. Rinse and leach for several days with conductivity water.
4. Repeat step 3.
5. Rinse and leach for several days using quartz distilled water.
6. Repeat step 5 and store until needed filled with quartz distilled water.

Typical analyses for the high purity solutions are given in Table II. Samples for analysis were prepared by evaporating 2 ml of the reagent in a teflon cone to a few hundred lambda using a heat lamp. (It was found that using leached quartz cones for this step sometimes

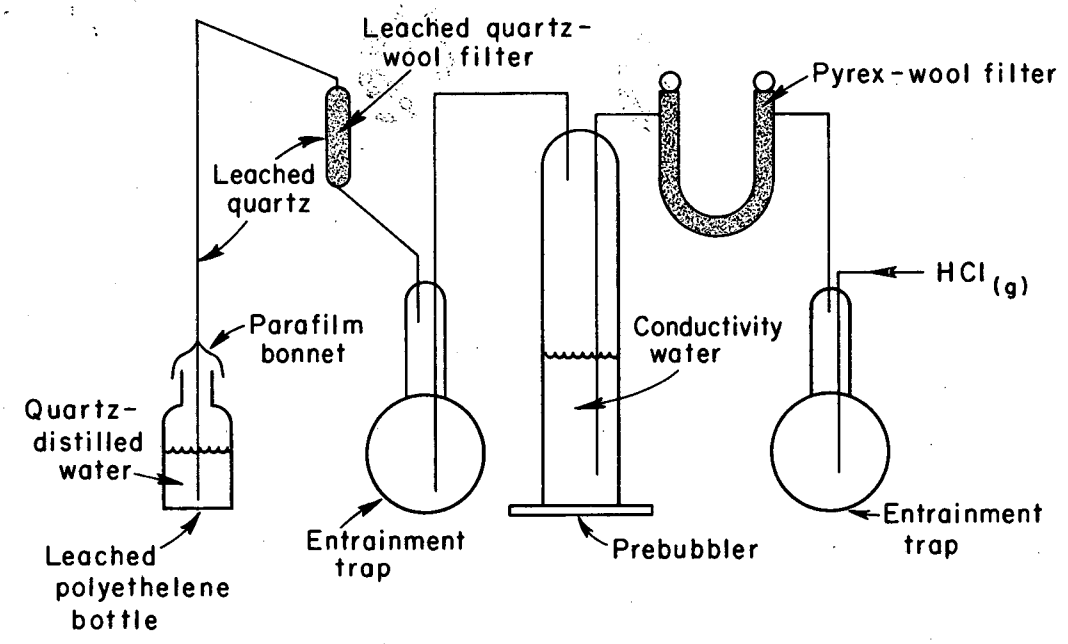

Fig. 1. Apparatus for the preparation of high purity HCl solutions.

introduced detectable quantities of Ca, Al and Si.) The concentrated samples were then placed on Cu electrodes and analyzed by emission spectroscopy. Several of these analyses were repeated after several months of storage to test the compatibility of the solutions and the containers. No detectable increase in contamination was noted.

c. High Purity Ion Exchange Resin. The first step in all the preparative procedures used in this study was the absorption of the californium product on beads of specially purified Dowex 50 x 4 cation exchange resin. Resin purification was achieved by washing commercially available BioRad AG 50 x 4 cation resin with conductivity water, 1 M HCl, 6 M HCl, saturated 20% alcoholic HCl, 6 M HCl, 1 M HCl, and finally with conductivity water. The ash content of the resin was then determined to be 4.3 ppm. Compared to the concentration of Cf in the resin phase after saturation, this level of contamination is negligible.

C. Ion Exchange Column Operation

The ion exchange techniques used in this study are essentially those which have become more or less standard in actinide purification chemistry.[7] The most significant differences that do occur are in scale and in the precautions taken to maintain high purity with respect to background contaminants.

Initial purification operations were primarily intended to remove gross primary contaminants. They involved the use of carrier precipitations, anion exchange columns, 2 M HCl cation cleanup columns[8,9] and alcoholic HCl columns.[10] If other actinide elements were present, a "but" column separation was performed.[11] It is worthwhile noting that, with the exception of decay products, recontamination by man-made actinides can not occur in a reasonably well controlled laboratory. During these operations, background contamination was not of particular concern; the glassware used was pyrex and the reagents were only of ordinary purity.

In the final stages of the purification, extensive precautions were taken to minimize background contamination. The product solutions contacted no surfaces other than specially cleaned quartz or small areas of carefully leached polyethylene (ion exchange column tips). The reagents used were high purity water and HCl solutions which had been spectroscopically analyzed.

Two techniques were used to monitor the column elutions. The first and most convenient was based on a small solid state alpha detector[12] which was positioned to count alpha particles emitted from the eluant drops as they built up on the tip of the column. This device provided an immediate indication of the californium concentration in the eluant with enough accuracy for efficient fractionation. This technique was not applicable to the very small columns because practical drop sizes were too large to allow accurate fractionation. In this case, small volume fractions were continuously collected on platinum plates and counted. Although less convenient, the data was essentially the same as presented by the drop counter.

The columns relied on most heavily for purification were the 2 M HCl cation cleanup column and the alcoholic HCl column. They were operated as follows:

a. Cleanup Column

1. The feed solutions were evaporated to dryness and then taken up in a minimum volume of 0.05 M HCl. This solution was then loaded on the pretreated column and rinsed in with a small volume of 0.05 M HCl.

2. 2 M HCl was then added and the elution continued to the first positive indication of alpha activity in the effluent.

3. The californium was then stripped by removing any excess 2 M HCl remaining above the resin bed and introducing 6 M HCl. The elution was continued until the product had been removed from the column.

b. Alcoholic HCl Column

1. The feed solutions were evaporated to dryness and taken up in a minimum volume of 0.05 M HCl. This solution was then loaded on the pretreated column and rinsed in with a small volume of 0.05 M HCl.

2. Approximately 2 free column volumes of 2 M HCl were then pushed through the column to minimize the perturbations to the band shape due to resin shrinkage.

3. Saturated alcoholic HCl was then added to the column and the product collected as before. The effectiveness of an alcoholic HCl column as a rare earth separation is known to be very sensitive to the concentration of HCl in the eluting solution.[13] For this reason, it was considered advisable to operate these columns with gaseous HCl above the solutions rather than air, particularly with the small scale separations. This ensured that the eluting solution remained saturated with respect to HCl at room temperature. The apparatus used in this procedure is shown in Fig. 2.

The method of preparation of the high purity columns was the same in both cases. Leached quartz columns were loaded with Dowex AG 50 × 4 ion exchange resin using leached quartz wool for retaining plugs above and below the resin columns. The resin was then washed by passing several free column volumes of high purity HCl solutions in the concentration sequence 2 M, 6 M, 12 M, 6 M, 2 M, 0.05 M.

The preparation of quartz glassware for high purity operations is of considerable importance; therefore, the procedure used for cleaning will be described.

1. The surfaces are initially cleaned with detergent in tap water and then soaked for several minutes in a concentrated detergent solution containing approximately 1% HF. This effectively removes contaminants adhering to the surface.

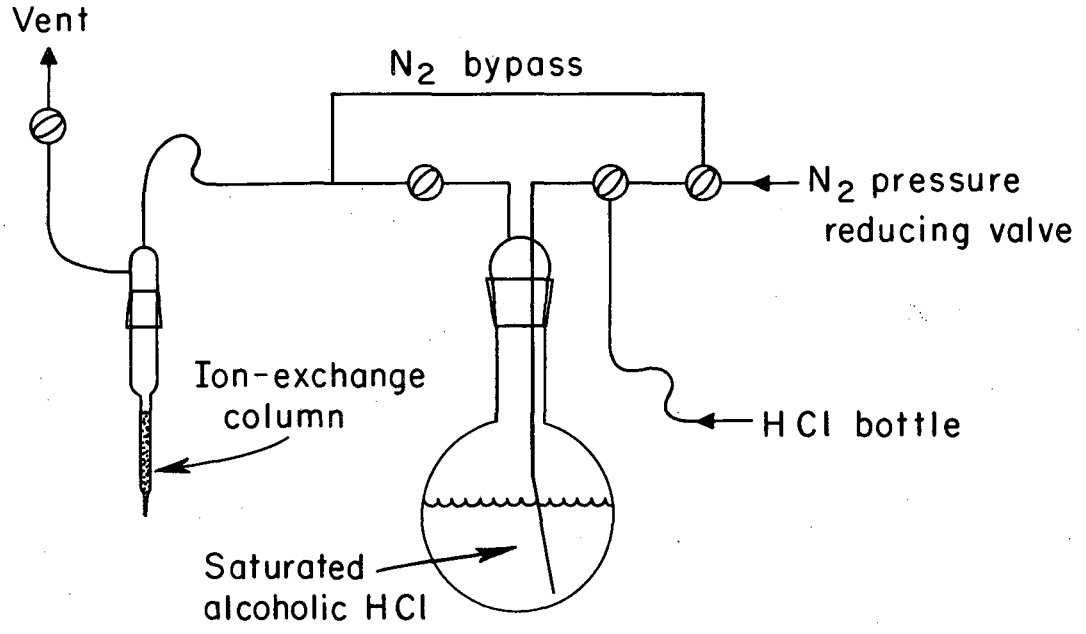

MU-36964

Fig. 2. Feed system for alcoholic HCl ion exchange columns.

2. The quartz is then placed in 6 M HCl made from C.P. concentrated HCl and conductivity water. The solution is brought to a brief boil and allowed to cool and stand for 12 to 24 hours. Care should be taken not to allow large volume decreases during boiling to prevent silica precipitation on the surfaces of the quartz. This has been noted on several occasions when 12 M HCl was used as the leaching agent. Presumably, the reagent HCl is the source of dissolved silica.

3. Following this, the pieces are rinsed and soaked for several days in conductivity water.

4. The apparatus is then given a final rinse and soaked until needed in quartz-distilled water.

D. Purification Operation Flowsheets

As has been mentioned previously, two complete purification cycles were carried out during this study. The details of these operations are presented schematically in the form of flowsheets in Figs. 3 and 4. With the exception of analytical information, these diagrams are self-explanatory and will not be discussed further.

E. Analytical Techniques

Due to the difficulties involved in the purification of small amounts of heavy actinides and to the danger of recontamination, it is essential that analytical procedures be developed to evaluate the purity of the preparations prior to their use. In order for an analytical technique to be useful in a study such as this, it is necessary that sample sizes be relatively small with respect to the total amount of material available. This results in the amounts of material handled being considerably smaller than in the purification operations; therefore, the sensitivity to recontamination is substantially increased.

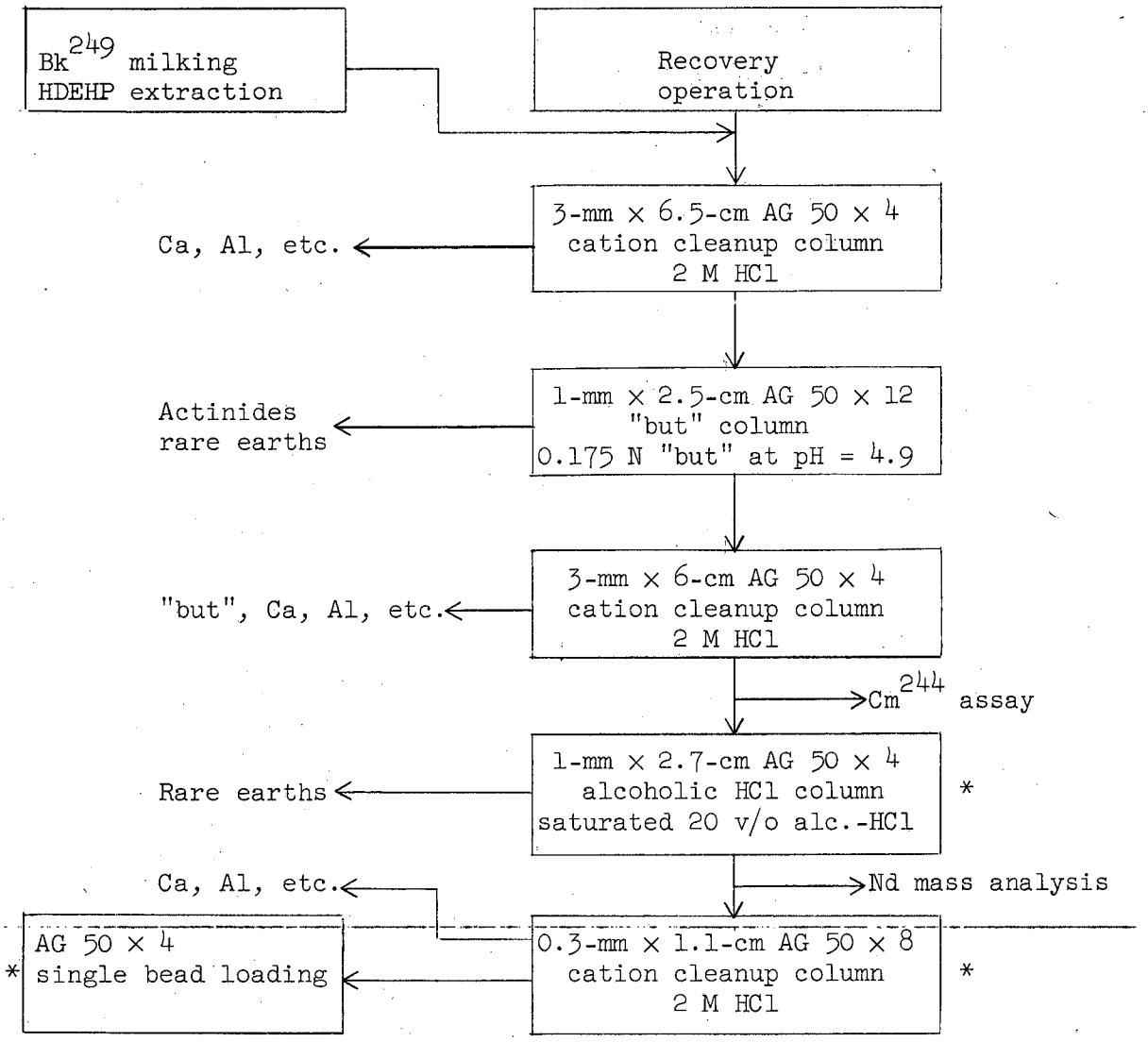

Fig. 3. First Cf^{249} purification cycle. The asterisk denotes high-purity operations carried out using leached quartz equipment and high-purity reagents.

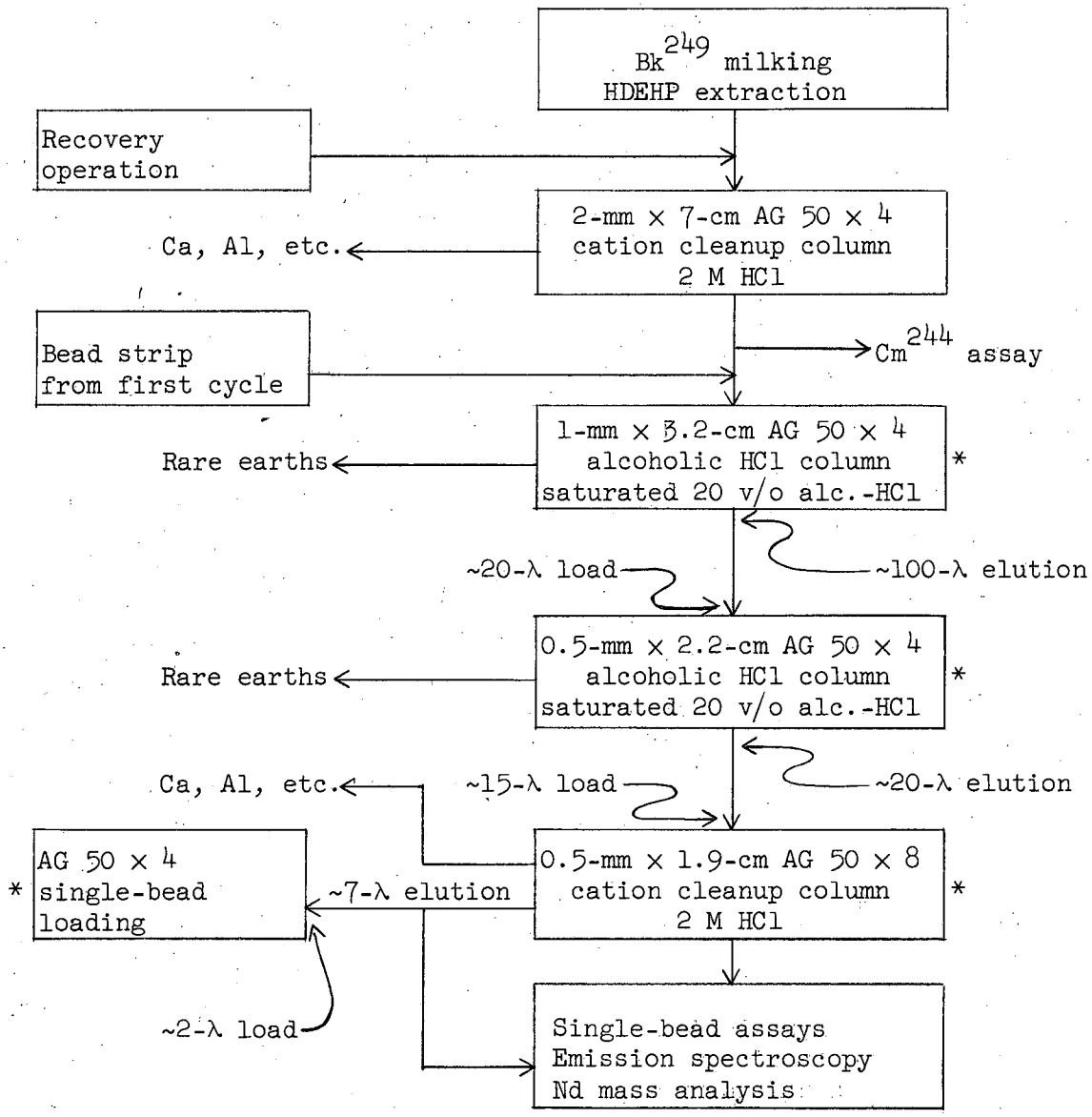

Fig. 4. Second purification cycle. The asterisk denotes high-purity operations carried out using leached quartz equipment and high-purity reagents.

This situation is mitigated to some extent by working with small volumes. This relieves the sensitivity to reagent purity and part of the sensitivity to contamination by homogenous surfaces; however, the effect of particulate contamination, i.e., dust, and localized surface impurities, is essentially independent of the volumetric scale and is, therefore of considerable concern.

For the reasons given above, obtaining meaningful analytical data is somewhat difficult; however, it should be noted that such analyses indicate upper limits for impurities in the sample.

1. Mass Analysis for Neodymium

Mass analysis is an extremely sensitive technique which is well suited to the quantitative determination of cations in very small samples. The method used is one of isotopic dilution[14] in which an isotopically enriched "spike" of the cation of interest is mixed with a sample of the unknown. Knowing the size of the sample, the amount of spike added and the isotopic composition of the spike and the mixture ordinarily allows the calculation of the concentration of the impurity in the sample. In order to be able to run mass analyses for a given cation, it is necessary to have an isotopically enriched spike, reagents of acceptable purity and a suitable electrode system. It is possible, in principle, to determine a large number of potential contaminants using this technique; however, these procedures are relatively expensive in terms of time and effort. It was, therefore, decided to check only the most troublesome of the potential contaminants, i.e., the rare earths. It was further assumed that the relative abundances of the rare earths were estimated average values for the earth's crust. It is unlikely that the abundances in the sample correspond to these values to any high accuracy; however, this assumption was considered adequate for the purposes of this study. The earth crust averages used are shown in Table III. The entire rare earth series was, therefore, related to neodymium, which is one of the more abundant members of the series and one for which mass analysis could be carried out

Table III. Rare earth abundances averaged over the earth's crust. (g/metric ton)[15]

La	19.0	Tb	1.0
Ce	44.0	Dy	4.3
Pr	5.6	Ho	1.2
Nd	24.0	Er	2.4
Sm	6.5	Tm	0.3
Eu	1.0	Yb	2.6
Gd	6.3	Lu	0.7

conveniently. It can be seen from Table III that the ratio of total rare earths to neodymium is approximately five. In order for these assumptions to be valid, it is necessary that the rare earth contaminants be derived from nature, i.e., have natural abundances and not have, for instance, fission product abundances. The isotopic ratios observed for Nd in the samples indicated that the source was indeed natural. One further concern is the possibility of chance contamination by an individual rare earth; however, the occurrence of such an event was considered to be unlikely.

Table IV shows the results of these analyses for both purification cycles. The rare earth content of the product from the first purification cycle was considered to be too large for the material to be of use either spectroscopically or crystallographically; therefore, when the results for these analyses were received, work was stopped and the second purification was run. The product from the second purification cycle was considered acceptable with respect to rare earth purity, within the assumptions mentioned above.

2. Actinide Analyses

Analyses for Pu, Am, and Cm were made by standard alpha pulse height counting techniques. No alpha peaks could be located other than those of the Cf isotopes known to be present. Upper limits for contaminating isotopes were computed from the ratio of the number of counts in the peak Cf^{249} channel to the maximum scatter in the counting data in the neighborhood of the energy corresponding to the major peak of the isotope of interest. These data together with the half life information necessary for the computation of limits of detection are listed in Table V.

Two isotopes of major interest, Cm^{244} and Pu^{242}, are not included in the above tabulation. Due to the long half-life of Pu^{242}, it was not possible to set meaningful limits from alpha counting data.

Table IV. Neodymium content of californium samples (mass analysis).

Sample	Sample size (ng Cf^{249})	Total Nd in unknown (atom %)	Estimated total rare earths (atom %)
Cycle I			
1	4.48	contaminated during analysis	
2	4.48	2.9	14.5
3	4.48	1.7	8.5
Cycle II			
1	8.66	0.32	1.6

Table V. Actinide analyses from alpha pulse height data.

Isotope	T 1/2 (yrs)	Maximum counts detected	Maximum content (atom %)
Pu^{238}	90 [16]	< 50	< 0.02
Pu^{239}	2.46×10^4 [16]	< 20	< 1.7
Pu^{240}	6.5×10^3 [16]	< 20	< 0.4
Am^{241}	458 [16]	< 50	< 0.08
Am^{243}	8×10^3 [16]	< 30	< 0.8
Cf^{249}	320 [17]	9×10^4	

The determination of Cm^{244} was considerably complicated by the fact that its major alpha peaks coincide almost exactly with major Cf^{249} peaks. The important features of the decay schemes of Cm^{244} and Cf^{249} are shown in Table VI. High resolution pulse height data was obtained in the region of 5.8 MeV. The composite peak was carefully decomposed into the component peaks in such a way that both components peaked at the proper energies and that both components had the same shape. The relative abundances of the two peaks may be related to the relative amount of Cm^{244} present in the following way.

Let

A_S = counts in 5.75 MeV peak
A_L = counts in 5.80 MeV peak
A_{Cm} = counts total Cm^{244}
A_{Cf} = counts total Cf^{249}
S_{Cm} = relative abundance of Cm^{244} in 5.75 MeV peak
S_{Cf} = relative abundance of Cf^{249} in 5.75 MeV peak
L_{Cm} = relative abundance of Cm^{244} in 5.80 MeV peak
L_{Cf} = relative abundance of Cf^{249} in 5.80 MeV peak

$$A_L = L_{Cm} A_{Cm} + L_{Cf} A_{Cf} \qquad (1)$$

$$A_S = S_{Cm} A_{Cm} + S_{Cf} A_{Cf} \qquad (2)$$

Also

$$\frac{\text{wt. Cm}}{\text{wt. Cf}} = \frac{A_{Cm}}{A_{Cf}} \frac{T_{1/2}\,(Cm)}{T_{1/2}\,(Cf)} \qquad (3)$$

combining (1), (2), and (3) and assuming wt. Cm $\ll$ wt. Cf.

$$\text{w/o } Cm^{244} = (100) \frac{T_{1/2}\,(Cm)}{T_{1/2}\,(Cf)} \frac{A_L S_{Cf} - A_S L_{Cf}}{A_S L_{Cm} - A_L S_{Cm}} \qquad (4)$$

Table VI. Alpha decay characteristics of Cf^{249} and Cm^{244}.

Cf^{249}(16) $T_{1/2} = 320 \pm 13$ yrs.(17)			
Alpha energy (MeV)	Relative abundance (%)	Alpha energy (MeV)	Relative abundance (%)
5.687	0.4	5.941	3.3
5.749	4.4	5.990	0.08
5.778	0.5	6.072	0.4
5.806	84	6.139	1.1
5.842	1.2	6.194	1.9
5.898	3		

Cm^{244}(17) $T_{1/2} = 18.11 \pm 0.07$ yrs.(18)	
Alpha energy (MeV)	Relative abundance (%)
5.661	0.017
5.759	23.3
5.801	76.7

Sample calculation:

$$(100)\ \frac{18.11}{320}\ \frac{(5.50\times10^{4})(0.044) - (2.90\times10^{3})(0.84)}{(2.90\times10^{3})(0.767) - (5.50\times10^{4})(0.233)}$$

$$= -0.10 \pm 1.0 \text{ w/o } Cm^{244} \qquad (5)$$

Because of uncertainties in the relative abundances of the Cf^{249} alpha groups and the analysis of the counting data, the absolute accuracy of these determinations is not particularly high and the limit of detection probably is no better than approximately 1% Cm^{244}. The results of the Cm assays ran less than these limits; therefore, setting a Cm^{244} limit of <1% is consistent with the accuracy of the method.

3. Emission Spectroscopic Analysis

Approximately 150 ng of the Cf from the final stage of the second purification cycle was submitted for emission spectroscopic analysis using copper spark excitation. The results of this determination are shown in Table VII. Because of the large limits of detection relative to the sample size, this analysis was of value only in demonstrating the absence of very gross contamination. No emission lines of any extraneous cations were detected with the exception of Be. The Be lines seen were far below the smallest quantitative standard available, which was 10 ng. The mass limit for the detection of Be is the lowest in the periodic chart, 0.2 ng[19]; therefore, it is estimated that approximately 0.2 ng of Be was present. Although only 0.1% by weight, this is almost 3 atom percent, demonstrating again the sensitivity of purity to materials of low atomic weight. The source of the Be is unknown; the cation cleanup column immediately preceding this analysis should have easily removed any Be in the preparation at that point. This probably is an excellent example of random background contamination.

Even though Be is known to be present in the solutions, the distribution coefficient for Be on Dowex 50 is considerably smaller than that for Cf;[20] therefore, it is reasonable to expect Be to be

Table VII. Results of emission spectroscopic analysis of the californium preparation in ng/150 ng Cf.

Ag < 10	Ge < 50	Sb < 500
Al < 10	Ho < 50	Sc < 10
Am < 100	In < 50	Si < 10
As < 500	Ir < 500	Sm < 50
Au < 500	K < 5000	Sn < 100
Be ~ 0.2	La < 10	Sr < 10
Bi < 50	Lu < 50	Ta < 500
Ca < 10	Mg < 10	Tb < 500
Nb < 50	Mn < 10	Th < 100
Cd < 500	Mo < 10	Ti < 50
Ce < 100	Na < 5000	Tl < 100
Cm ND	Nd < 100	Tm < 50
Co < 50	Ni < 10	U < 100
Cr < 10	Np < 1000	V < 10
Dy < 50	Pa ND	W < 100
Er < 50	Pb < 10	Yb < 10
Eu < 10	Pr < 500	Y < 10
Fe < 50	Pu < 500	Zn < 500
Ga < 10	Re < 100	Zr < 10
Gd < 50	Rh < 50	

efficiently excluded from the resin phase during bead loadings, assuming an excess of Cf in the aqueous phase at equilibrium. For this reason, such an excess was maintained during all bead loading operations.

4. Single Ion Exchange Bead Assays

The most sensitive technique used for the determination of overall purity was a single ion exchange bead assay which was originally suggested by Dr. J. C. Wallmann. Basically, this method involves the determination of the total capacity of a single ion exchange bead by the saturation and elution of a high purity alpha active material of known half-life. The calibrated bead is then saturated in a sample of the final product solution. Since the actinide must compete with impurity cations for absorption sites in the resin, the amount of activity absorbed is a direct measure of the overall purity of the product on ion exchange beads. The first step in all of the preparative procedures used in this study is the absorption of the californium on single resin beads; therefore, this assay has the advantage of measuring the purity of the product in the same form in which it will be used. Like other assay methods, this provides no information on the nature of the impurities; however, it is sensitive to the number of equivalents of impurities, independent of the masses of the atoms.

The counting data from the assay may be related to the total equivalent percent contaminants in the product by the following argument.

If

C = bead capacity in equivalents

X = equivalents of impurities absorbed on the bead

T(S) = half-life of the tripositive actinide standard

T(Cf) = half-life of Cf^{249}

R(S) = alpha count rate in strip from bead calibration

R(Cf) = alpha count rate in strip after Cf absorption

Then

$$\frac{R(Cf)}{R(S)} = \frac{T(S)}{T(Cf)} \quad \frac{C-X}{C} \tag{6}$$

or rearranging

$$\frac{X}{C} = 1 - \frac{R(Cf)}{R(S)} \quad \frac{T(Cf)}{T(S)} \quad \frac{\text{equivalents impurities}}{\text{equivalents total}} \tag{7}$$

or combining (6) and (7)

$$\frac{X}{C-X} = \frac{T(S)}{T(Cf)} \quad \frac{R(S)}{R(Cf)} - 1 \quad \frac{\text{equivalents impurities}}{\text{equivalents Cf}} \tag{8}$$

The standard used for this work was Am^{241}. This particular isotope was chosen because it has an accurately known half-life which is comparable to that of Cf^{249}, and it was readily available in the form of a pure stock solution. The half-life for Am^{241} used in these calculations was 458 yrs.[15]

The scale of the assay was set at approximately 10 ng to allow 2π counting of the complete elution samples. The following is a practical description of the technique used for these assays:

1. A high purity Dowex 50 × 4 ion exchange bead with a capacity of approximately 10 ng was introduced into the tip of a clean quartz microcone.
2. Approximately 100 ng of the Cf to be analyzed was taken up in 1 λ of 0.05 N HCl and added to the bead.
3. The bead and solution were equilibrated for 30 minutes and then separated by pipetting. Following this, the bead and cone were rinsed with a 1 λ portion of quartz distilled water.
4. After the removal of the rinse, 10 λ of 6 N HCl was added and equilibrated with the bead for 30 minutes. The solution was then removed and plated on a platinum counting planchet. This procedure was repeated with another 10 λ of 6 N HCl.

5. The bead was then loaded with Am^{241} and subsequently stripped and plated using the same technique described for the californium.

Associated with this determination are several potential sources of uncertainty which should be mentioned. Probably the most serious problem and the most difficult to avoid is the sensitivity of the small analytical sample to contamination. The sample size used in this particular analysis was 50-100 ng of californium. The contents of a fleck of dust introduced into the sample could be enough to invalidate the results of any subsequent assay. Without further study and development, this point alone makes it advisable to consider the bead assay results as setting an upper limit for impurities. Another potentially important difficulty involves the retention of extraneous activity from the loading step as contamination on the walls of the microcone. The cone and bead were rinsed between the loading and stripping operations; but it is very difficult to guarantee that the small volume water rinse adequately cleaned all of the contaminated surfaces that are contacted by the larger volume of strip solution. This error would probably be reflected as scatter between results for duplicate analyses. Extraneous activity could also be held up during the loading step by the retention of free solution within the porous structure of the bead. Even if one assumes, however, that the rinsing procedure is ineffective, the low concentration of material in the aqueous phase ($\sim 5 \times 10^{-4}$ M) compared to the high concentration in the resin phase (~2 M) makes the extraneous activity from this source negligible with respect to the activity absorbed on the bead.

It is probable that the distribution coefficients for Am and Cf will drop rather drastically with close approach to saturation in the resin phase. In order to use the bead assay technique, it is necessary to assume that, under the conditions used, the deviation of the resin from saturation is negligible or that the degree of saturation is the same for Am and Cf. Both of these assumptions should be valid;

however, neither have been investigated experimentally. It is also conceivable that radiation damage could cause changes in the distribution coefficients or in the bead capacity during the assay. This effect is probably of no concern with Cf^{249}; however, with materials of high specific activity, the problem could become a major one.

It should also be noted, that the absorption on the bead of an alpha active material with a half-life smaller than Cf^{249} would tend to cancel the effect of absorbed inactive materials. To avoid this problem, it is always advisable to independently analyze for other alpha emitters.

The accuracy with which the half-lives of Am^{241} and Cf^{249} are known will directly effect the accuracy of the method. The half-life for Am^{241} is well known; however the half-life of Cf^{249} is known only to ±4%.[17] Further, the method is inherently limited by the accuracy of alpha counting techniques, which under most conditions are not reliable to more than 1-2 percent.

This analysis was done in duplicate on a sample of the californium product from the second purification cycle. The procedure was also carried out using Am^{241} in both absorption operations to test the reproducibility of the method. The results of these analyses are shown in Table VIII. These data show a scatter of approximately 10% which is probably due, in large part, to variable amounts of extraneous activity from contamination of the walls of the microcone during loading.

The californium results make it clear that relatively large amounts of contaminants are potentially present. The all-inclusive nature of the assay make it impossible to identify impurities directly; however, since a large excess of Cf was present in the aqueous phase during bead loading, it is necessary that the impurities have distribution coefficients comparable to that of Cf in order to be absorbed in the resin phase to any major extent. This argument in addition to considerations of the relative abundances of possible impurities allows one to list the "most probable" identity of the contaminating species, i.e., other tripositive actinides, lanthanides, Al and Ca. Mass analysis

Table VIII. Single bead assay results.

Bead	Bead capacity (c/min) Am	Cf	Total impurities (eq./eq. Cf^{249})
1	42133	43800	0.37
2	79400	86160	0.32
3	57609	-	-
3 (reload)	52330	-	-

excludes the rare earths as major contaminants. Counting data eliminates the other actinides with the exception of Pu which is eliminated as a possibility by absorption spectra data to be presented in Sec. III. Further, the analytical data accumulated during the development of the high purity HCl solution preparation and previous experience with operations similar to those involved here indicate very strongly that the most difficult contaminants to control are Al and Ca. Although it is not possible to be definitive, by any means, it is felt that the most reasonable choices for the most probable contaminants are Al and Ca. It should also be noted that due to their low atomic weights, relatively small masses of these materials account for the observed impurity levels; for instance, approximately 4 weight percent Al in Cf constitutes 35 equivalent percent contamination.

In summary, Nd contamination has been set at 0.32 atom % and total rare earths have been estimated at approximately 1.6 atom %. Cm^{244} has been set at <1 atom %, Am set at <1 atom % and, although it is not possible to set a quantitative limit for Pu, it is felt that chemical and spectroscopic evidence indicates its absence. Purity with respect to these materials is reasonably certain and acceptable; however, the bead assays indicate the possible presence of considerable amounts of other materials. Chemical and relative abundance arguments lead to the tentative identification of the most probable contaminants as Al and Ca. It should be noted, however, that crystallographic evidence is not consistent with gross contamination of the samples.

III. ABSORPTION SPECTRA OF Cf^{+3}

During the course of this study, several sources of californium were prepared that could be used for the observation of absorption spectra. Techniques were devised which allowed spectra to be recorded from saturated cation exchange resin beads, both singly and in multi-bead stacks, from a sample of hydrated californium chloride and from a small single crystal of $CfCl_3$.

A. Spectrum of Californium Absorbed on Cation Exchange Beads

Single particles of Dowex 50 x 4 cation exchange resin are smooth, spherical, transparent beads. When saturated (5.2 milliequivalents capacity/dry gram of resin) these beads constitute a mechanically stable and relatively highly concentrated sample. For instance, in the case of a trivalent cation such as californium, the concentration in a saturated bead is approximately 2 M. Previous work done in this laboratory by Cunningham and Wallmann[2,3] has demonstrated the possibility of using these beads as microabsorption cells for obtaining the spectra of absorbed cations. The technique developed at that time consisted of locating a saturated single bead in a close fitting hole punched in a platinum disk as shown in Fig. 5. This unit was then placed under a microscope and the spectrum observed in a hand spectroscope positioned to accept the magnified image of the bead. Although the technique was amply demonstrated using other materials, the absorption spectrum of Cf^{+3} was never observed. A similar experiment was done during this study. A single bead approximately 90 microns in diameter and containing approximately 200 ng of Cf^{+3} was selected from the beads loaded after the first purification cycle. This was placed in a mask, Fig. 6, and the spectrum was observed through a microscope fitted with a 10x objective and having the ocular replaced with an Atago direct vision hand spectroscope. The light source used was a tungsten filament

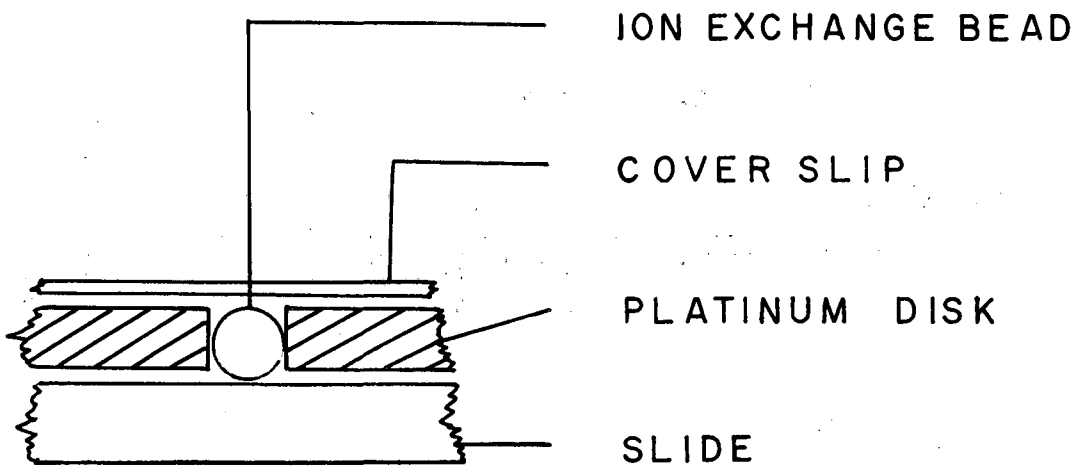

MU-22115

Fig. 5. Single bead microabsorption cell developed by Cunningham and Wallmann.

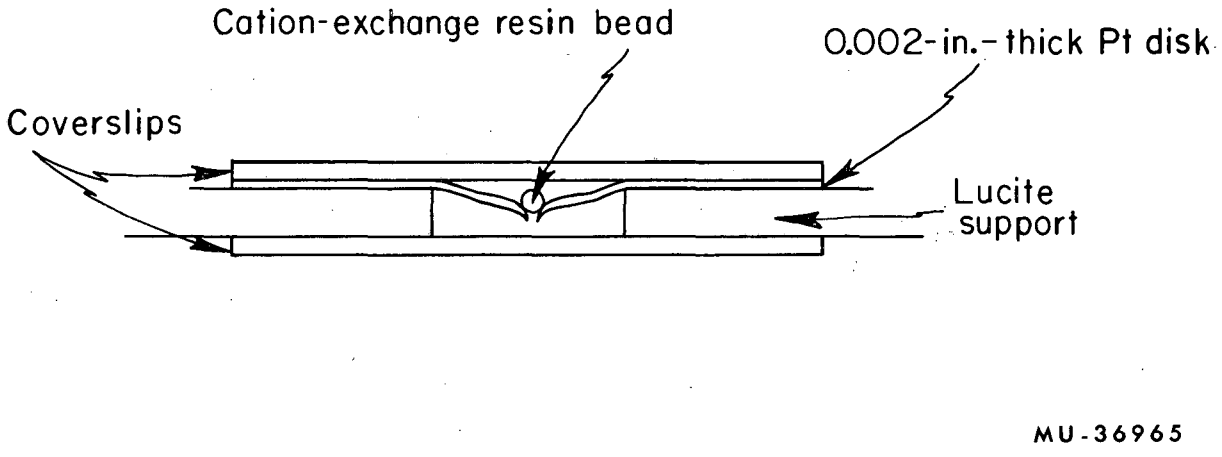

Fig. 6. Single bead microabsorption cell used in this study.

microscope substage lamp focused on the sample by means of a substage condenser. Visually, an absorption line was clearly observed by several people at 473 mμ. The author and R. D. Baybarz independently observed additional lines at 493, 596, and 610 mμ; however, the intensity of these lines was so low that their existence could not be positively demonstrated.

The encouraging results obtained using the single bead prompted the development of a technique by which spectra could be taken through a multibead stack. This procedure allowed substantial intensification of the spectra. A sketch of the microabsorption cell used is shown in Fig. 7. One problem that is exaggerated by stacking is the loss of light due to scattering out of the primary beam. Optically, the resin beads function as very short focal length spherical lenses which cause the transmitted light to be focused very divergently immediately above the beads. This difficulty was avoided, in part, through the use of a quartz light pipe which was allowed to press on the top of the stack. This served to insure optical contact between the beads and also acted as a light gathering device which covered a considerable solid angle above the top bead. The light source used in these experiments was a 100 watt concentrated Zr arc lamp manufactured by Sylvania Electric Products, Inc. This source had a high intensity; however, some difficulty was caused by the occurrence of prominent arc lines in some spectral regions. In order to allow permanent recordings to be made of the spectra and also to extend the accessible spectral region beyond the visible, the apparatus shown in Fig. 8 was assembled for photographing the spectra. Photography was carried out using a Polaroid Land Camera with Type 3000 film for the visible region and Type 47 film for the infrared region.

The wavelength scale in the hand spectroscope was calibrated on each exposure by simultaneously photographing a Hg arc reference spectrum adjacent to the absorption spectrum and the superimposed image of the scale. The spectral features in the visible region were

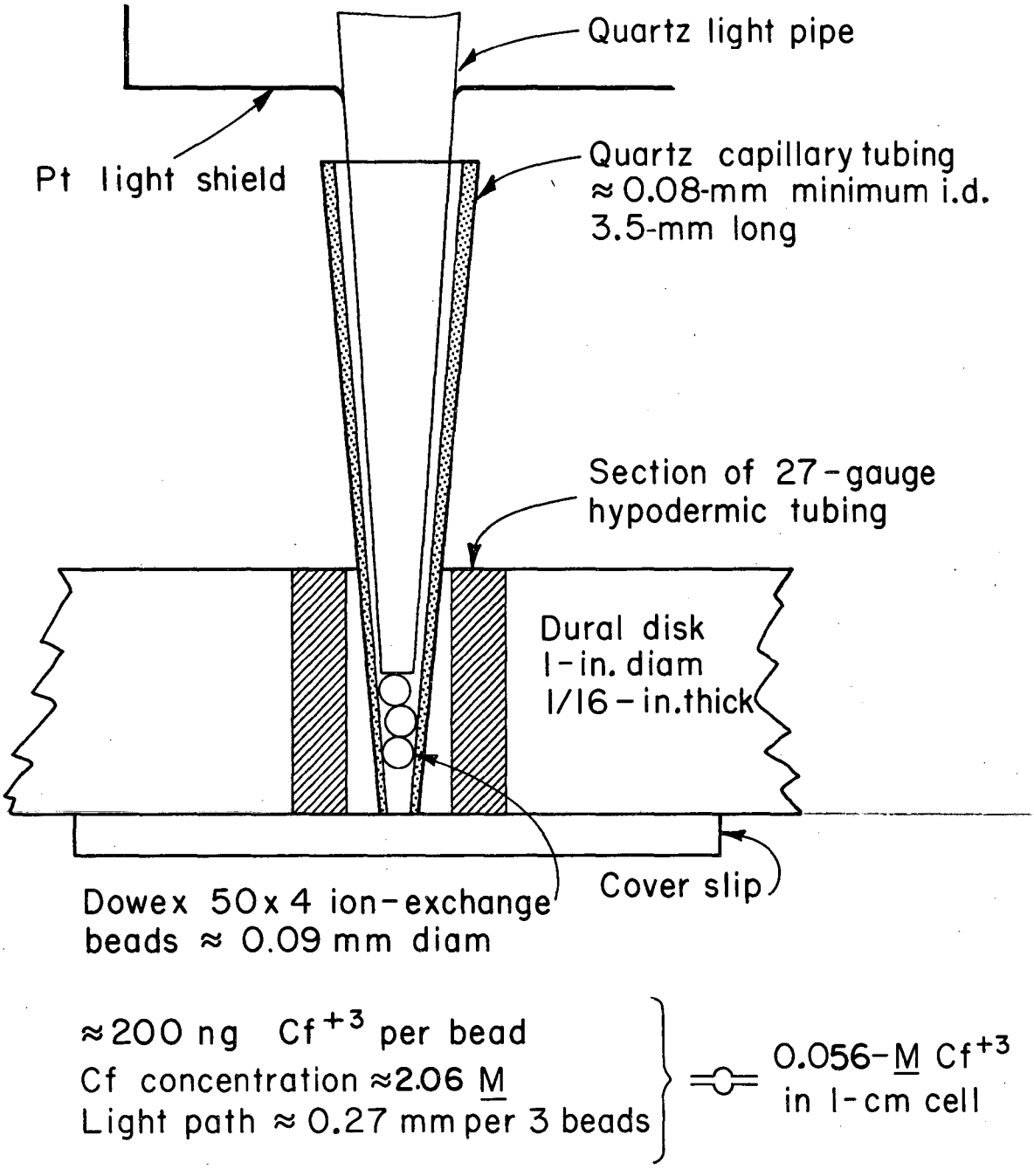

Fig. 7. Stacked bead microabsorption cell.

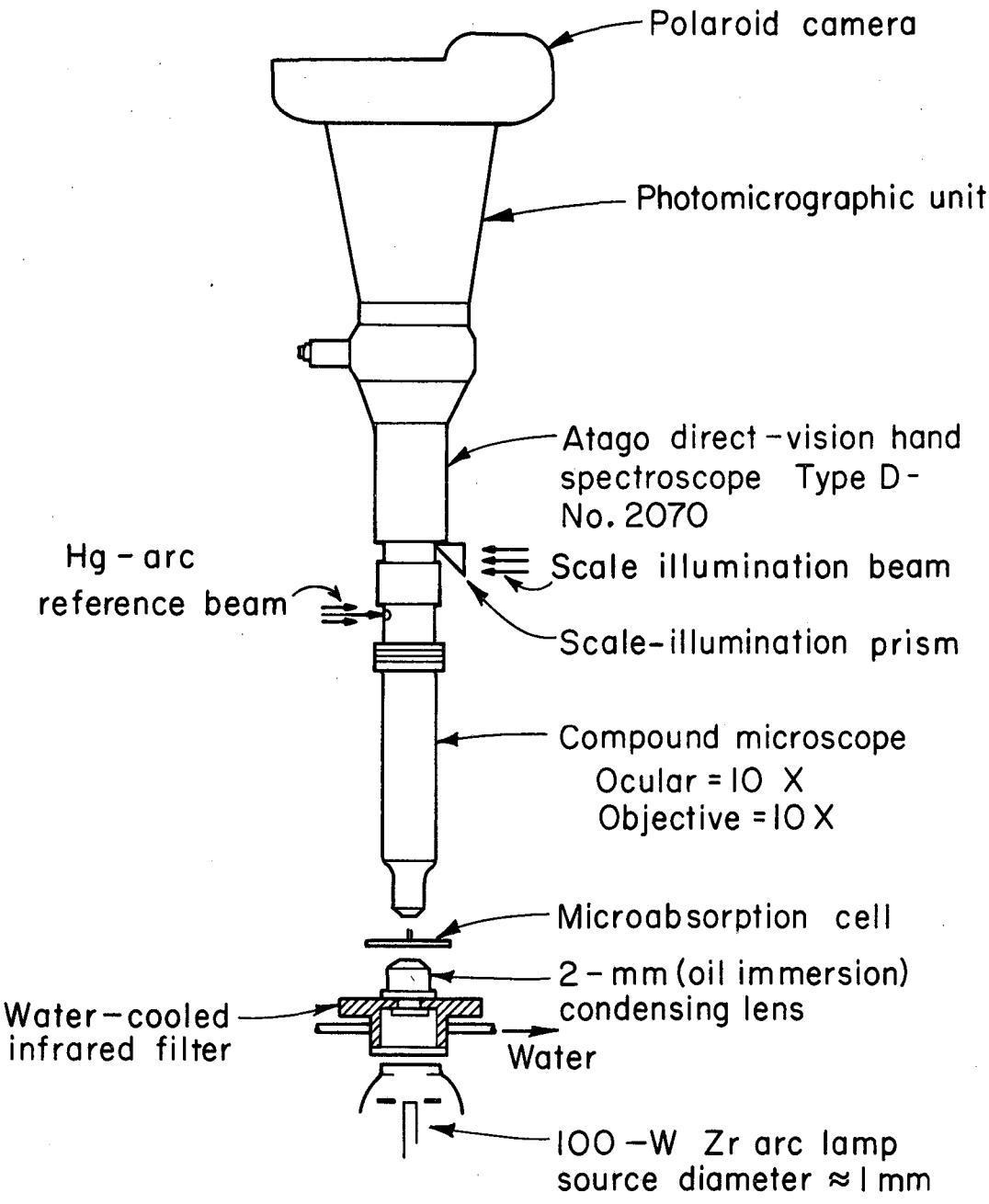

Fig. 8. Apparatus for photographing spectra through a hand spectroscope.

reproduced several times within experimental error using material from both purification cycles. The infrared region was observed only during the work done using the material from the second purification. A line list and line description for spectra obtained after the second purification are given in Table IX.

A parallel experiment was run using beads saturated with praseodymium. A line list in the visible region for Pr^{+3} on a bead stack is given in Table X, which also includes published data on the solution spectrum. These data show that, at least in the case of Pr^{+3}, line positions in the bead spectra are not appreciably shifted with respect to those in solution. Less precise observations on Nd^{+3} and Pu^{+3} indicate that this is also the case for these ions. Based on this information, the positions of the absorption lines for Cf^{+3} in solution are presumed to be close to those observed in the bead experiments.

The estimation of extinction coefficients is a difficult problem for two reasons. First, from the qualitative description of the Pr bead spectra, it is possible only to say that the relative intensities of the lines are consistent with the relative solution extinction coefficients and second, the comparison of the Cf bead spectra and the Pr bead spectra is limited to visual estimation from the polaroid photographs. Within the bounds of these limitations, estimated extinction coefficients for Cf^{+3} in solution are given in Table XI. It is felt that these estimates should be considered very approximate.

B. Spectrum of Hydrated Californium Trichloride

During the bead loading operation after the second purification cycle, the evaporation of a chloride solution containing a total of approximately 6 μg of californium yielded a sample of what is presumed to be hydrated californium trichloride. This material was obtained in the form of a clump of clear, emerald green crystals located in the tip of a small quartz microcone. The absorption spectrum of this preparation

Table IX. The absorption spectrum of Cf^{+3} absorbed on Dowex 50 cation exchange resin.

Peak position (mμ)	Extent (mμ)	Qualitative Description
473 ± 2	469-475	strong
491 ± 2	489-493	weak and relatively sharp
591 ± 2	590-618	visual observation indicated two lines; however, photographically often only one moderately strong line at 593 mμ was apparent
595 ± 2		
605 ± 2		weak to moderate
620 ± 3	-	very weak—existence uncertain
645 ± 3	638-650	weak
675 ± 3	670-680	moderate
no structure	720-760	strong

Table X. The absorption spectrum of Pr^{+3} absorbed on Dowex 50 cation exchange beads with solution data for comparison.

Solution[21]		Bead stack	
Position[a] (mμ)	ϵ[a]	Position (mμ)	Description
444	9.1	443 ± 2	strong-broad
469	3.6	468 ± 2	medium-moderately broad
483	3.6	483 ± 2	medium-sharp
589	1.9	587 ± 3	weak-broad

[a]Data for chloride solution

Table XI. Approximate molar extinction coefficients for Cf^{+3} in solution estimated from Cf^{+3} and Pr^{+3} bead data as compared to Pr^{+3} solution data.

Peak position on beads (mμ)	Estimated molar extinction coefficients
473	5 - 10
491	1 - 2
591 + 595	2 - 4
605	2 - 4
645	1 - 2
675	2 - 4
720 - 760	5 - 10

was photographed in the visible region with the apparatus used for the stacked bead experiments (Fig. 8) with the microcone replacing the microabsorption cell. Because of the large amount of californium involved, the spectrum was very intense and easily photographed. A list of lines observed during this experiment is shown in Table XII. These data show, for lines observed in both systems, that the bead spectrum and the hydrated chloride spectrum are virtually identical. The band from 425 mμ to 450 mμ had not been observed previously because insufficient light was transmitted through the bead stack in this region to allow photographic recording.

C. Absorption Spectrum of Californium in a Single Crystal of Anhydrous $CfCl_3$

From a theoretical standpoint, it is very desirable to have absorption data for californium in a crystalline matrix which is similar to the $LaCl_3$ matrix in which the lighter actinides have been studied. This allows direct comparisons to be made between the various parameters used in fitting the experimental data.

During the course of the preparation of $CfCl_3$ samples for crystallographic studies, a single crystal of $CfCl_3$ was prepared. Physically, the sample was a clear, emerald green, more or less spherical particle which was approximately 35 microns in diameter. The sample was prepared and subsequently contained in a thin quartz x-ray capillary. The details of the preparation and a crystallographic description of the sample are given in Sec. IV.

In as far as technique was concerned, a major problem involved the construction of a suitable light mask for the sample. The system which was developed for this purpose is shown schematically in Fig. 9. The unit consisted of a pair of razor blades positioned edge to edge in such a way as to constitute a combination positioning trough and a one dimensional slit mask with a separation slightly less than the

Table XII. Absorption spectrum of californium in hydrated californium chloride.

Peak position (mμ)	Description
425 to 450	Strong absorption but no structure observable due to Zr arc line interference.
473	strong
490	weak
595	moderate
610	moderate

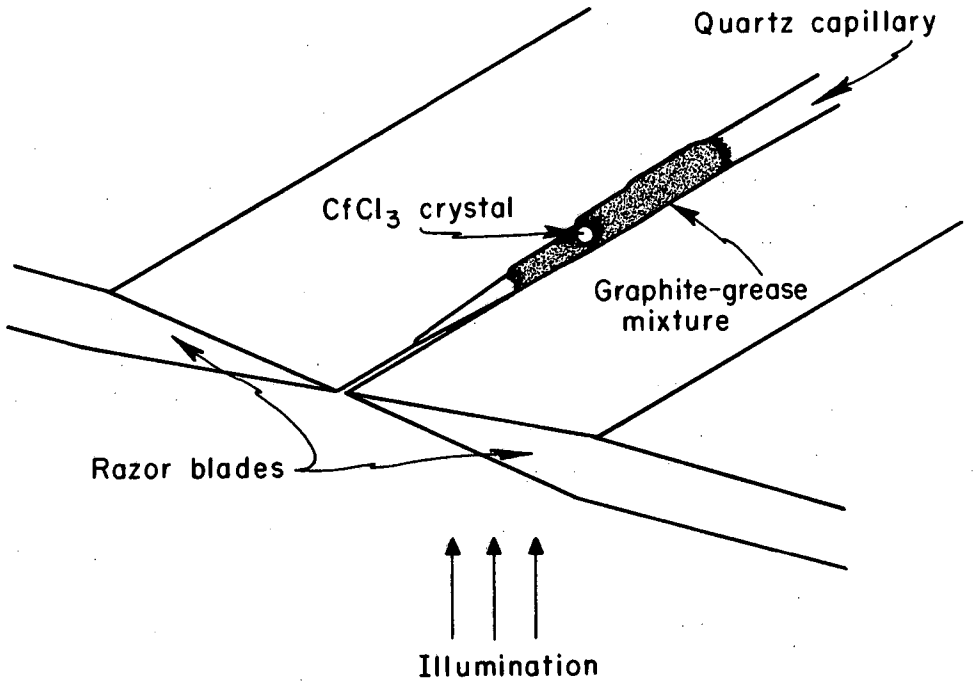

Fig. 9. Microabsorption cell for $CfCl_3$ crystal.

diameter of the bead. Masking along the slit was achieved by the application of an opaque graphite-grease mixture along the length of the capillary. This mixture was also used to repair light leaks due to the noncoincidence of the sample position and the plane of the slit. The masking paint was prepared by the evaporation of a colloidal graphite-water suspension (Aquadag) to dryness and redispersion of the graphite in Apiezon L vacuum grease by grinding. This material was satisfactory optically; however, there was an annoying tendency for thin layers to creep and either obscure the sample or allow light leaks to form. Subsequent experience has shown that the use of glycerine in place of the grease yields a mix that is more satisfactory from this standpoint.

The spectrum of this sample was photographed using the apparatus described earlier, Fig. 8. A line list compiled from this experiment is given in Table XIII. The general structure of the spectrum is very similar to that observed in the ion exchange bead and hydrated chloride experiments; however, shifts in line position have occurred.

For theoretical analysis of the spectrum it is necessary to obtain enough data of sufficient accuracy and resolution to allow a least squares fit of the data to a mathematical model. In order to be reasonably meaningful, six parameters should be fitted, i.e., the Slater radial integrals, F_2, F_4, and F_6, the spin-orbit-radial integral, ζ_{5f}, and the configuration interaction parameters α and β. To be statistically significant, more spectral data was required than was obtained using the hand spectroscope. For this reason, it was decided to attempt to extend the accessible spectral region and to improve resolution and accuracy by recording the spectrum using a high speed grating spectrograph. The general configuration of the apparatus used is shown in Fig. 10. The spectrograph was a 3 meter, f6.3, Model 75-000 Jarrel-Ash fitted with a 15000 line per inch grating blazed for 7500 A. The plate dispersion at first order under these circumstances was approximately 20 A/mm. Using this apparatus, it was possible to extend the wave length region from approximately 4000 A to approximately 10,000 A.

Table XIII. Absorption lines of $CfCl_3$ crystal photographed through the hand spectroscope.

Peak position (mμ)	Description
483 ± 2	strong - broad
500 ± 2	weak - sharp
582 ± 2[a]	trace - very sharp
615 ± 2	moderate to strong - broad
630 ± 3	moderate - sharp
665 ± 3	moderate - broad
690 ± 3	moderate - broad
740 - 770	strong - possible structure

[a]Line due to Nd impurity

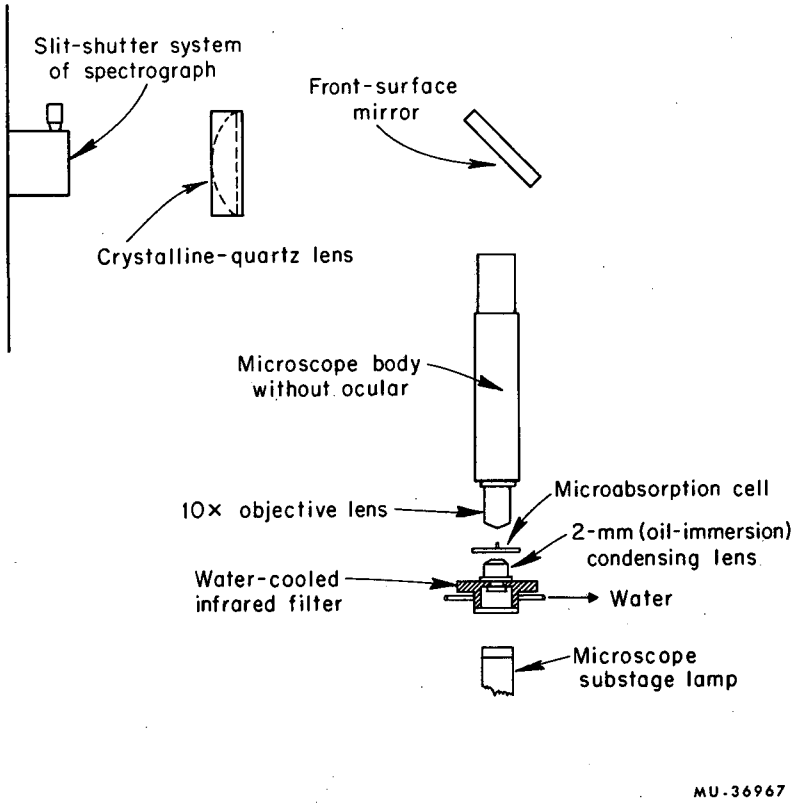

Fig. 10. Apparatus used to record absorption speatra on a grating spectrograph.

The limitation at long wavelengths was imposed primarily by the speed of available photographic emulsions. The limitation at short wavelength was due to the unavailability of a source with a sufficiently intense output below 4000 Å to allow exposures to be taken with this apparatus in a reasonable length of time. The source used throughout this phase of the investigation was a simple tungsten filament microscope substage lamp operated at approximately 50% voltage overload. A Hanovia 150 watt high pressure Xe arc lamp[22] was used in an attempt to extend the wavelength region deeper into the ultraviolet region. This source was substantially more intense at lower wavelengths compared to the tungsten filament; however, the decrease in output of the lamp with decreasing wavelength or a sharp decrease in transmission of some component in the system limited its use to wave lengths above 3500 A for reasonable exposure times, i.e., a day. In principle, it would be possible to extend the spectrum considerably deeper into the ultraviolet by using very long exposure times, ie.e, a week; however, the steep gradients in optical density in the region of useful exposure on the plate would result in the location of absorption features on very steep shoulders making them very difficult to detect or locate with any accuracy.

The experimental method used in this study was deficient in one major respect; it could be used only at room temperature. Thermal broadening prevented good resolution of the fine structure of the spectrum. It should be possible to construct cryogenic and optical systems which would allow spectra to be taken at liquid He temperatures; however, time did not permit the construction of such an apparatus during this study.

Multiple exposures of the spectrum with adjacent Hg arc reference spectra were taken using glass spectrographic plates of a type appropriate to the wavelength region covered, i.e., 4000-6500 A, Type 1-F; 6000-9000 A, Type 1-N; 7000-10,000 A, ammonia hypersensitized Type 1-M.[23] The plates were densitometered using a Jarrel-Ash Model

2310 console comparator microphotometer. Densitometer tracings of several different exposures of the same region were made to define the reproducible features of the spectra and then permanent records were made of the two best exposures in addition to the matching reference spectra. The positions of peak maxima and emission lines were then located on the tracings by measurement from plate edge reference marks. A dispersion factor curve for a particular tracing was then computed from the measurements of the reference spectrum. These data in conjunction with the measurements from the tracing of the absorption spectrum allowed the computation of the wavelengths corresponding to peak maxima. The location of a point on the tracings could be done considerably more accurately than the maxima of the absorption peaks could be marked; therefore, errors in measurement did not contribute significantly to the overall error in the location of absorption maxima. It should be noted that no attempt was made to separate incompletely resolved components. Minor absorption features positioned on the tail of larger peaks were located by marking the centers of the shoulders. The positions of these features are, therefore, somewhat approximate. Relative peak intensities were arrived at by visual comparison. A list and description of the absorption features observed in this experiment are given in Table XIV. The trace lines located at 5837 A and 8043 A[24] coincide closely with strong absorption lines of Nd^{+3} in $LaCl_3$. The observed intensities of these lines are consistent with the amount of Nd known to be present in this preparation; therefore, these two lines were ascribed to Nd and not considered as part of the Cf^{+3} spectrum. Other Nd lines with intensities comparable to the lines observed occur in the spectral region investigated; however, they occur in regions where Cf absorptions are observed. The californium lines are very much more intense than those to be expected from Nd and would, therefore, be expected to completely obscure the neodymium lines if they did occur. No consistent correspondence could be made between the observed spectrum and the spectra of the other actinides or lanthanides.

Table XIV. Absorption spectrum of a single crystal of anhydrous $CfCl_3$ photographed using a grating spectrograph.

Peak position (A)	Error limits (A)	Description of components	Relative intensity of band
4304	5	major peak	
4383	5	small shoulder	moderate-broad
4505	5	small shoulder	
4579	5	small shoulder	
4828	5	major peak	strong-moderately broad
5005	5	major peak	weak-sharp
5837[a]	5	trace	trace-very sharp
6148	5	major peak	
6237	10	minor shoulder	moderate-broad
6295	10	medium shoulder	
6678	5	large shoulder	weak-broad
6872	5	major peak	
7539	5	major peak	strong-moderately broad
7764	5	major peak	strong-broad
8043[a]	5	trace	trace-very sharp
8546[b]	5	major peak	
8734[b]	10	minor shoulder	weak-broad
8907[b]	10	minor shoulder	

[a]Lines ascribed to Nd impurity.

[b]Only one useful exposure available; therefore, the measurement of peak positions was not done in duplicate.

Dr. Katheryn Rajnak has carried out a preliminary analysis of the crystal data using theoretical techniques which have been applied to the spectra of many of the rare earths and several of the lighter actinides.[25-27] The fitting technique has been treated in detail elsewhere; therefore, it is appropriate here only to very briefly indicate the basis for the procedure.[28]

The energy level structure of the $5f^5$ configuration was determined by calculating the effects of interelectronic repulsion within the configuration and spin-orbit interactions using a first order perturbation treatment based on a central field approximation in the zeroth order. The perturbing Hamiltonian is

$$\mathcal{H}' = \sum_{i=1}^{N} \left[-\frac{Ze^2}{r_i} - U(r_i) \right] + \sum_{i<j}^{N} \frac{e^2}{r_{ij}} + \sum_{i=1}^{N} \xi_i \vec{l}_i \cdot \vec{s}_i \qquad (9)$$

The energy level structure within the configuration is affected only by the last two terms; therefore, matrix elements involving only the more abbreviated Hamiltonian

$$\mathcal{H}' = \sum_{i<j}^{N} \frac{e^2}{r_{ij}} + \sum_{i=1}^{N} \xi(r_i) \vec{l}_i \cdot \vec{s}_i \qquad (10)$$

need be considered. Further, the indicated summation need be carried out only over the electrons in incompletely filled shells since the inclusion of electrons in closed shells serves only to shift the energy of the configuration as a whole by a constant amount. The elements of the energy matrix associated with these perturbations may be shown to have the form

$$E = \sum_{k=0}^{3} e_k E^k + A \zeta_{5f} \qquad (11)$$

where the coefficients e_k are associated with the angular part of the interelectronic repulsion interaction and the E^k are parameters which

may be related to the Slater radial integrals F_k. The coefficient, Λ, is also associated with the angular part of the spin-orbit interaction while ζ_{5f} is the spin-orbit radial integral defined as

$$\zeta_{5f} = \int_0^\infty R_{5f}^2 \, \xi(r) \, dr \qquad (12)$$

Further, it should be noted that in the case of an f^n configuration E^o, as is also the case with F_o, depends only on the number of electrons in the unfilled f shell and, therefore, the term $e_o E^o$ serves only to shift the configuration as a whole without altering its structure. This parameter is included; however, it is defined such that it shifts the energy level diagram as a whole so that the algegraic sum of the residuals is zero.

In order to adequately describe the energy level schemes of the rare earths and actinides it has often been found necessary to include the effect of coulombic interactions between electrons in different configurations. These interactions occur only between configurations having the same parity and differing in the coordinates of not more than two electrons. The parity of a configuration is defined as even or odd depending on whether the sum of the one electron orbital angular momenta are even or odd; for instance, $5f^5$ may interact with $5f^4 7p$ but not with configurations such as $5f^4 6d$ or $5f^4 7s$. The description of the energetics of this interaction has been investigated using second order perturbation theory where it has been shown that if the interacting configurations are well separated, this effect may be accounted for by the addition of a correction to the first order electrostatic interaction term.[29] This procedure results in the addition of three more terms to the elements of the energy matrix

$$\alpha \, L(L+1) + \beta \, G(G_2) + \gamma \, G(R_7) \qquad (13)$$

where α, β, and γ are treated as parameters and $G(G_2)$ and $G(R_7)$ are quantities derived from group theoretical considerations. The coefficient $G(R_7)$ is a function of the seniority of the state. Since all of the observed low lying levels have the same seniority and are, therefore, effected by the same amount, the inclusion of this term in the matrix elements is not necessary. This results in final matrix elements involving 6 coefficients e_1, e_2, e_3, Λ, $L(L+1)$ and $G(G_2)$, which may be evaluated from theoretical considerations, and 7 quantities, E^0, E^1, E^2, E^3, ζ_{5f}, α, and β, which are treated as parameters. From a practical point of view, the fitting technique involves the assignment of experimentally observed transitions to the appropriate levels within the configuration and then the use of fast computer techniques, to fit the parameters in such a way as to give the best least squares fit to the experimental data.

Since the data were taken at room temperature, the individual crystal field components of the J-levels were not resolved. It was necessary, therefore, to assume that the measured peak centers were the centers of gravity of the individual J-levels. In addition, at room temperature, all or most of the crystal field components of the ground state term, $^6H_{15/2}$, are populated; therefore, the observed peaks include transitions from excited crystal field components as well as the ground state. This probably results in the observed peak center having a lower energy than the true center of gravity of the upper J-level. However, this is a semisystematic error and would not be expected to greatly effect the relative separations of the J-levels. One further problem is that it is not possible to experimentally determine the center of gravity of the ground state term. This was arbitrarily set at 100 cm^{-1} for the purposes of the calculations. The error involved in this assumption is probably no larger than errors associated with the location of the other levels. Initial energy level calculations were carried out using values for E^1, E^2, E^3, ζ_{5f} and α which were estimated by linear extrapolation from the corresponding parameters

for U^{+3}, Pu^{+3}, and Np^{+3}. The data for U^{+3}[30] and Np^{+3}[31] are somewhat tentative while the Pu^{+3}[32] data are well established. On the basis of these computations, trial assignments were made and least squares fitting calculations were carried out. Computations of this type resulted in the assignments shown in Table XV. The energy level values calculated from the results of the least squares fit based on these assignments are also shown in Table XV. The parameters resulting from the fitting calculations are shown in Table XVI. Using 7 parameters to fit 10 levels, the rms deviation was computed as the square root of the sum of the squares of the individual deviations divided by the number of levels fit minus the number of parameters used. This was computed to be 170 cm^{-1} for the final fit which is certainly as good as could be expected. The final values for the E^k and ζ_{5f} parameters are of the order of 5% smaller than predicted by the extrapolation from the lighter actinides. β was found to be approximately the value estimated by extrapolation; however, α was almost a factor of 2 smaller than expected. α and β have rarely been included in similar calculations and it is, therefore, not certain that they exhibit a linear variation with atomic number. Further, it should be pointed out that the data from this study is for Cf^{+3} in a matrix of $CfCl_3$ while the data used for comparison was derived from diluted materials in $LaCl_3$ or $LaBr_3$ matrices. A small increase in covalent bonding in $CfCl_3$ as compared to $LaCl_3$ or $LaBr_3$ could account for the observed trends in E^k and ζ_{5f}. This observation is consistent with the smaller radius of Cf^{+3}, which, presumably, would tend to increase the covalent character of the Cf-Cl bonds. The significance of these observations is somewhat obscured by the tentative nature of the U^{+3} and Np^{+3} calculations.

The most serious uncertainty involved in the calculations is the assignment of J values to the observed transitions. Since no experimental data is available which allows the independent evaluation of J values, it is necessary to make assignments only on the basis of agreement with calculation. Since it is difficult to evaluate the degree

Table XV. Results of a 7 parameter least squares fit of absorption data for Cf^{+3} in a matrix of $CfCl_3$.

2 J	Peak position Observed (A)	Observed (cm^{-1})	Calculated (cm^{-1})	Difference (cm^{-1})
15		100[a]	124	24
11			6755	
13			7760	
9			7876	
11	8546	11700[c]	11655	45
9	7764	12880	12853	27
3	7539	13260	13237	23
7			14063	
7	6872	14550	14625	125
5	6678	14970	15036	76
15	6148	16260[c]	16094	166
5			16778	
1			17374	
5	5005	19970	19921	49
17	4828	20710	20890	180
11	4579	21830	21783	47
21			22014	
19			22203	
9	4505	(22190)[b]	22166	(24)
3	4383	(22810)[b]	22762	(48)
13	4304	(23230)[b]	23242	(12)
7			23419	
11			24937	

[a] Estimated level.

[b] Not used in fitting calculation.

[c] Major peak used in fitting calculation—minor peaks considered as resolved crystal field components.

Table XVI. Spectroscopic parameters resulting from least squares fit of $CfCl_3$ data.

E^0	19990		cm^{-1}
E^1	4711.5	± 9	cm^{-1}
E^2	15.9	± 0.1	cm^{-1}
E^3	414	± 1	cm^{-1}
ζ_{5f}	-3467	± 4	cm^{-1}
α	40	± 1	cm^{-1}
β	-2580	± 55	cm^{-1}

of sophistication of present theoretical treatments, it is not possible to say when the extent of agreement between observed and calculated levels proves that the level assignments are correct. These uncertainties would be most easily resolved by crystal absorption data taken at low temperature. This being the case, such measurements should clearly be an early objective for future spectroscopic studies of californium. It may well be, that further information will lead to the reassignment of some of the levels observed in this work; however, it is felt that such changes will be relatively minor and should not have a drastic effect on the parameters derived from this calculation. These results will at least, provide a better starting point for future calculations on the heavy actinides than the currently available hydrogenic parameters.

In as far as the bead data are concerned, sufficient experimental information is not available to allow fitting calculations to be made. The data that are available, however, are consistent with the assignments made for the crystal data with relatively minor changes in the parameters. A predicted energy level diagram for Cf^{+3} in solution has been calculated by Fields, Wybourne and Carnall.[33] These calculations were based on values of ζ_{5f} and F_2 extrapolated from solution data for the lighter actinides and on the assumption that the F_4/F_2 and F_6/F_2 Slater radial integral ratios are hydrogenic. A comparison of the energy levels predicted by this calculation and the data from the bead experiments does not indicate the existence of a statistically meaningful correlation. Both the order and relative separations of the levels differ markedly from those derived from the present calculation. In addition to the predicted energy levels, the above authors presented a graphical tabulation, in an energy level diagram, of experimental data available on Cf^{+3}. It should be pointed out that several of the points were transcribed directly from a line list of fluorescence transitions.[34] These data should not be included in such a tabulation since fluroescence transitions need not always involve the ground state.

IV. COMPOUND PREPARATION AND CRYSTALLOGRAPHIC STUDIES

A. Compound Preparations

The single ion exchange bead microtechniques are applicable to the preparation of a variety of compounds. The saturated organic resin bead is first converted to an oxide by air ignition. Other compounds may then be prepared from this sample by the use of appropriate anhydrous conversions.

1. Bead Ignition

The apparatus used for the conversion of the saturated resin bead to an oxide is shown in Fig. 11. The resin bead is picked up on a fine platinum wire and, using micromanipulators, is introduced into the cavity in the platinum rod. Using a microtorch, the rod is then slowly heated. The bead goes through several distinctive changes in appearance during the ignition. As soon as the temperature gets high enough to begin to decompose the organic material, the surface of the bead becomes a very shiny jet black. It is during this stage of the procedure that the temperature must be most carefully controlled; if heating is too rapid, the bead will explode. At approximately 600°C the final amounts of organic material are burned away and the bead loses the shiny appearance and the color changes to that of the "sulfate". It is also at this point that the most abrupt volume changes occur; the diameter of the bead shrinks to about half of its original value. After these changes have occurred, the rate of heating may be increased substantially. As the temperature increases, the sample is converted through a rather complex series of sulfate compounds until at approximately 1200-1250°C the conversion to the oxide is complete.[35] In the case of californium, the saturated resin bead was a light yellow-green and the color of the "sulfate" and oxide phases was a pale yellow.

After the ignition, the oxide bead is transferred to a freshly dried quartz x-ray capillary drawn on the end of a specially cleaned quartz standard taper joint. The apparatus used for the transfer is shown in Fig. 12. During the removal of the microtorch and platinum

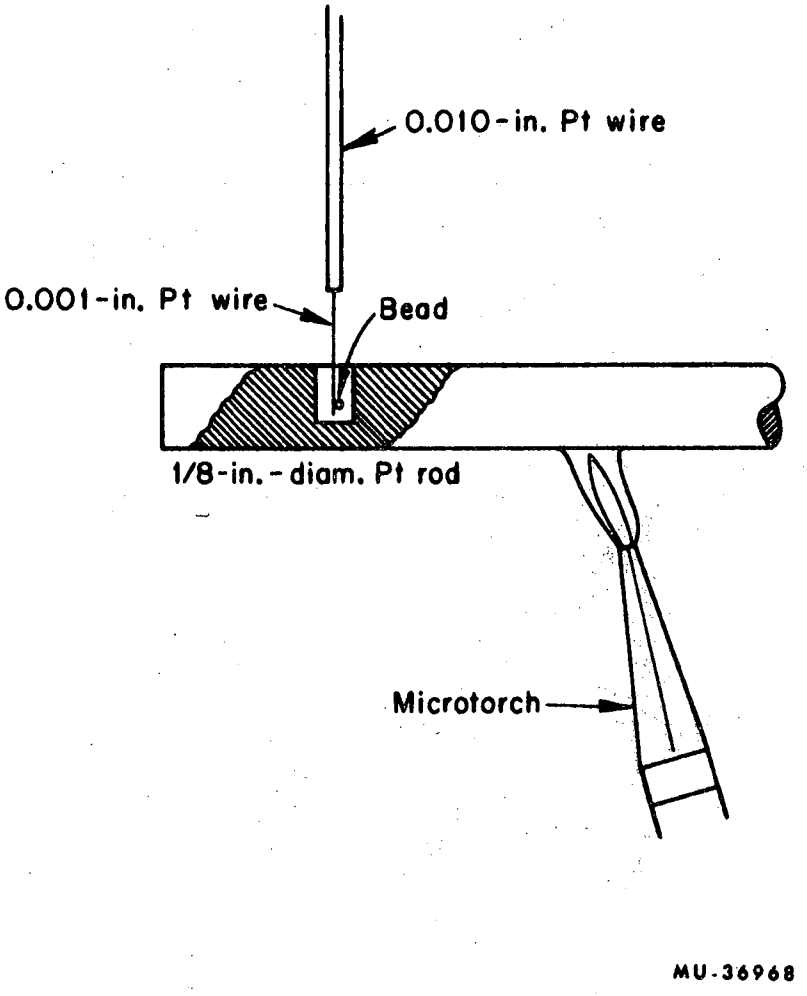

Fig. 11. Bead ignition apparatus.

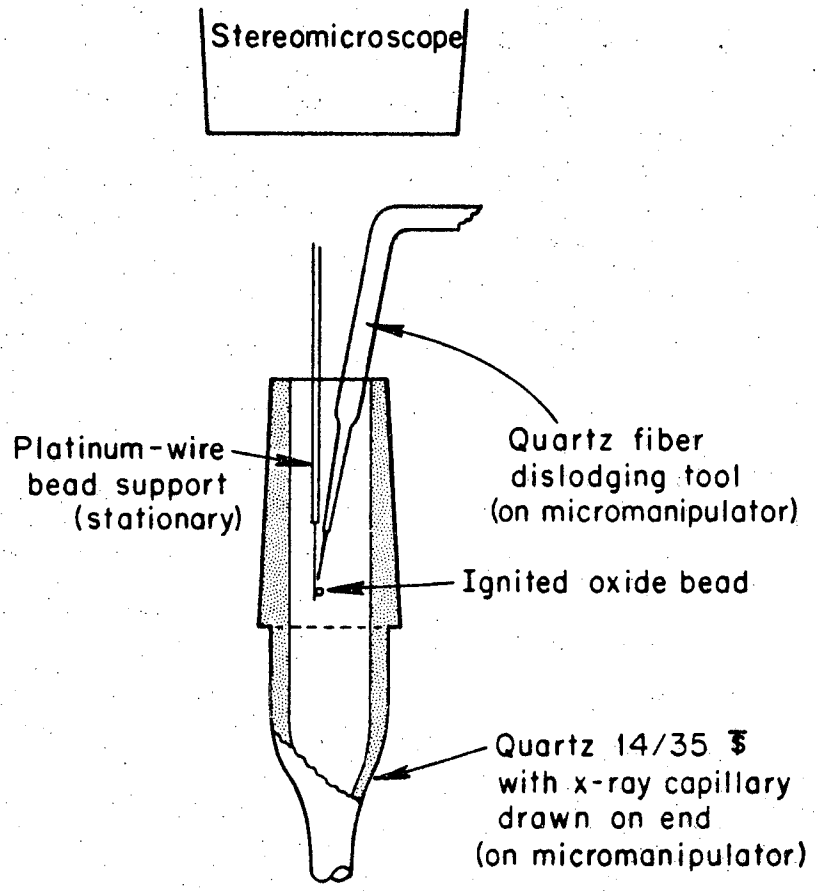

Fig. 12. Apparatus for transferring ignited oxide bead to x-ray capillary.

rod, and the assembly of the transfer equipment, the bead support assembly is held stationary to avoid inadvertently dislodging the bead. The scale of the preparations carried out in this study was approximately 200 ng of Cf. Resin beads containing this amount of material at saturation have a diameter of about 90 microns when dry; therefore, the diameter of the oxide bead after ignition is approximately 45 microns. The capillaries were drawn in such a way that the oxide bead would wedge into place about 2 mm back from the sealed tip. The wall thickness of the capillaries was maintained at 5 to 10 microns to minimize film darkening due to scattering from the quartz when the x-ray exposures were made.

2. Californium Sesquioxide

Samples of californium sesquioxide were prepared by hydrogen reduction of the air ignited oxide. The precise definition of the stoichiometry of micropreparations is a difficult problem. Since the samples are much too small to analyze directly, it is necessary to argue by analogy. The preparation of samples of Pr_2O_3 and Am_2O_3 with reasonably well defined stoichiometries have, for instance, been prepared from higher oxides using reduction conditions similar to those used in this study.[36] On the other hand, the system Pu-O is known to behave in a rather complex way in the neighborhood of $PuO_{1.5-1.6}$.[37] Oxides in which the cation exhibits mixed oxidation states, i.e., oxides in which appreciable departures from stoichiometry occur, are typically quite dark in color. Both the reduced and unreduced californium oxides prepared during this study, however, were quite light in color. The compound prepared is considered to be Cf_2O_3; however, it must be borne in mind that deviations in stoichiometry are possible.

The apparatus used in the preparative work in this study is shown in Fig. 13. The hydrogen used was obtained by the thermal decomposition of uranium hydride. The procedure used for the reduction is given below.

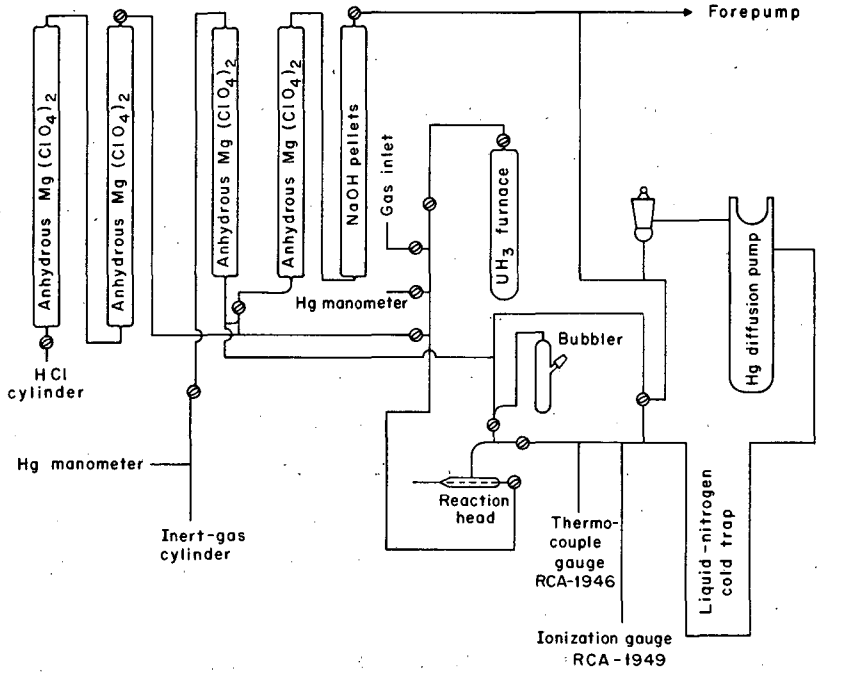

Fig. 13. Preparative vacuum line.

1. The capillary containing the air ignited oxide was placed on the vacuum line and evacuated to 10^{-6} mm Hg.
2. The system was vented up to 380 mm H_2 and the sample heated to 600°C for 20 minutes.
3. The system was evacuated to 2-3 × 10^{-6} mm at room temperature and then vented up to 380 mm H_2 and heated at 600°C for 20 minutes.
4. Step 3 was repeated.
5. The sample was cooled to room temperature and sealed off in 380 mm H_2.

The appearance of the samples was unchanged from that of the air ignited oxide.

3. Californium Trichloride

The californium trichloride samples were made by the treatment of the sesquioxide preparations with anhydrous HCl gas. After the x-ray examination of a Cf_2O_3 sample was complete, the capillary was opened and rejoined to the vacuum line using an Apiezon W wax seal. A technique of this sort allows the preparation of several compounds using the same material.

As was mentioned previously, there is some concern, about the possible presence of Al and Ca in the samples. The chloride preparation was used as an auxiliary purification step. The volatility of Al_2Cl_6 is such that heating to 500-600°C in vacuum after chlorination should effectively remove any Al present unless extremely stable solid solutions are formed. The removal of Ca under these conditions, however, is rather doubtful because of the much lower volatility of $CaCl_2$.

The source of HCl gas was preparative grade tank HCl. The procedure used for the hydrochlorination is given below.

1. The sesquioxide sample was heated in vacuum at 520°C for 10 minutes.
2. After cooling, the system was vented to 1 atm. with HCl. The sample was heated to 520°C and held for 10 minutes with an HCl flow through the upper end of the capillary taper.

3. Step 2 was repeated twice more.

4. The system was evacuated to 1×10^{-6} mm, heated to 520°C and held for 5 minutes.

5. The capillary was sealed off in vacuum.

During the first preparation, the chloride was heated to 600°C. The sample melted and on cooling, formed what appeared to be a single crystal of $CfCl_3$. This was the sample used during the spectroscopic studies. All subsequent preparations were not heated above 520°C. A single crystal was a clear emerald-green color, while the polycrystalline samples were a lighter green.

B. Crystallographic Investigations

The preparative techniques used in this study are somewhat unique; however, the equipment and procedures used for obtaining the diffraction patterns of the samples differ only slightly from standard methods. The differences that do occur are a consequence of the very small amounts of material used in the preparations. Because of the small size of the samples, the intensity of the diffracted beam is quite low and it is, therefore, important to minimize background radiation due to incoherent scattering and to the radioactivity of the sample. In a properly designed and assembled camera, the principal source of incoherently scattered radiation is the capillary used to contain the sample. The mass of quartz in the primary beam was minimized by using the very fine, thin capillaries described earlier. It is further possible to use microcollimation techniques; however, this was not found to be necessary. The decay of Cf^{249} results in the emission of alpha particles and a relatively small amount of gamma radiation. The alpha particles emitted by the sample were easily absorbed by thin filters located inside the camera. It is possible to minimze the effect of the gamma radiation from the sample by minimizing the exposure time through the use of high intensity x-ray equipment.

The x-ray generator used was a Model 80-000 Jarrel-Ash Microfocus unit manufactured under license from Hilger and Watts, Ltd. This apparatus was fitted with a copper anode and a focusing cathode assembly which produced a 100 micron by 1.4 mm line focal spot on the anode. The diffraction patterns were recorded photographically using a 57 mm diameter Phillips-Norelco precision powder camera in conjunction with Illford Industrial G x-ray film. A 0.0003 in. nickel foil filter was placed inside the camera to remove the copper β x-rays and any alpha particles penetrating the capillary. Typical exposure times using this equipment were 15-20 hours. The films were measured on a Phillips-Norelco film reader which has a precision of 0.05 mm.

The films used were independently measured in duplicate and the observed θ values averaged. The patterns were then indexed by comparison with data available on isomorphic compounds and through the use of $\sin^2 \theta$ and intensity calculations done using the POWD computer program developed by D. K. Smith.[38] The lattice parameters were computed by least squares fitting of the $\sin^2 \theta$ data using the LCR-2 program developed by D. E. Williams.[39] This program uses weighting factors of the form

$$w_i = \frac{\text{constant}}{\sin^2 \theta_i \, (\Delta\theta_i)^2} \qquad (14)$$

where $\Delta\theta$ is the random error in the measurement of θ, as estimated by the experimenter. $\Delta\theta$ was assigned a value of 0.05 degrees for all observed lines. When several calculated lines of comparable intensity fell very close to an observed line, the observed line was considered to be a superposition. In this case, each set of possible indices was entered into the lattice parameter computation using a $\Delta\theta$ modified in such a way as to give each component within the group a weight proportional to its calculated intensity and such that the effective $\Delta\theta$ for the whole group was 0.05 degrees. It has been found that using precision cameras and very small samples essentially eliminates errors due

to eccentricity and absorption; therefore, no extrapolation functions were used in the fitting.

In the modern crystallographic literature, it is common practice to report lattice parameters with probable error limits, 50% confidence, based on the internal consistency of a single preparation. Such error limits indicate that another determination of the lattice parameters using the same sample and identical equipment and techniques would have a 50% probability of yielding lattice parameters within the stipulated limits. Chemically, however, a much more valuable piece of information is the probability that another group of samples prepared using independent chemical and crystallographic techniques would yield average lattice parameters which would fall within a given set of error limits. Such an evaluation is necessarily divorced from the internal consistency of a single determination; it must be based rather on the consistency of a number of determinations using different preparations. In this case, the statistical treatment called for is one familiar to students of analytical chemistry.[54] Standard deviations are calculated as

$$\sigma = \frac{t}{\sqrt{N}} \sqrt{\frac{\Sigma(d_i)^2}{N-1}} \qquad (15)$$

where σ represents the error limits, for a given confidence level, based on the average of N independent determinations of the lattice parameters. The d_i are the deviations of lattice parameters for the different determinations from the average of the group. The factor t, commonly referred to as the Student t value, is included to account for the effect of nonstatistical sampling, i.e., the effect of using only a limited number of observations. The value of t is very sensitive to the number of observations, for instance, to 95% confidence, the value of t is 12.71 for 2 determinations, 4.30 for 3 determinations, and 1.96 for a very large number of observations.

Such a treatment is not suggested simply in the interest of conservatism. Statistically significant differences found to occur between groups of determinations, handled in the same way crystallographically, would strongly indicate the operation of unanticipated physical and chemical effects. It is felt that information of this type would be of great assistance in the recognition of anomalies due to the effect of purity, nonstoichiometry, radiation damage, annealing conditions, etc.

This sort of statistical treatment has been applied to the average lattice parameter results reported in this work. The Student t values used were chosen for 95% confidence. Since this treatment of crystallographic data is somewhat unorthodox, it should be pointed out that the error limits reported are considerably broader than would ordinarily be used. Error limits computed in this way are not comparable to those based on considerations of the internal consistency of a single determination; the broader limits reported here for average lattice parameters should not, therefore, be used as indications of the precision of the data from a particular sample. Information on internal consistency is presented in the form of $\pm 2\sigma$ limits computed in the usual way using least squares fitting calculations on the data from a single determination.

1. Californium Sesquioxide

Diffraction data on three Cf_2O_3 samples were recorded and analyzed. The structure in all cases was the monoclinic Sm_2O_3 type[40] exhibited by the sesquioxides of Pm,[41] Sm, Eu, and Gd. The lattice parameters computed for each sample are shown in Table XVII. A comparison between observed and calculated $\sin^2\theta$ and intensity data is given in Table XVIII. Statistically, the fit to the experimental data appears to be acceptable for the individual films and, as a group, the patterns are self-consistent. From a chemical point of view, however, it is felt that these data should be regarded as somewhat preliminary primarily because of the open questions involving the purity of the preparations.

Table XVII. Californium sesquioxide lattice parameters—monoclinic Sm_2O_3 structure.

Film number	a (A)	$2\sigma a$ [a] (A)	b (A)	$2\sigma b$ [a] (A)	c (A)	$2\sigma c$ [a] (A)	β (deg.)	$2\sigma\beta$ [a] (deg.)
2338A	14.132	0.011	3.592	0.002	8.811	0.007	100.31	0.07
2363A	14.122	0.008	3.591	0.002	8.807	0.006	100.32	0.06
2382A	14.116	0.008	3.590	0.001	8.808	0.005	100.31	0.05
average [b]	14.124 ±	0.020	3.591 ±	0.003	8.809 ±	0.013	100.31 ±	0.02

[a] Estimated standard deviation for the individual preparations as computed from least squares fits using the LCR-2 lattice parameter program.

[b] The error limits placed on the average values were computed using

$$95\%\ \text{confidence error limit} = \frac{4.30}{\sqrt{N}} \sqrt{\frac{d_i^2}{N-1}}$$

where d_i is the deviation of the individual lattice parameters from the average; N is the number of observations, i.e., 3; and the factor 4.30 is the 95% confidence Student t value for 3 observations.

Table XVIII. Line list and indexing for monoclinic californium sesquioxide—Film 2363A.

hkl	$\sin^2\theta$ Calculated[a]	$\sin^2\theta$ Observed	Intensity Calculated[b]	Intensity Observed[c]
111	0.0588	0.0589	8.0	10
401	0.0642	0.0641	8.5	9
$40\bar{2}$	0.0668	0.0665	9.1	9
003	0.0712	0.0711	6.4	8
310	0.0738	0.0736	10.0	9
$11\bar{2}$	0.0773	0.0773	9.5	10
600	0.1108	0.1106	1.2	4
$51\bar{1}$	0.1221	0.1221	1.9	5
$31\bar{3}$	0.1291	0.1287	4.3	7.5
313	0.1609	0.1609	5.4	7.5
020	0.1843	0.1836	2.8	6
$80\bar{1}$	0.1907	0.1908	1.6	4.5
$71\bar{2}$	0.2038	0.2037	3.5	6.5
404	0.2041		1.1	
$40\bar{5}$	0.2117	0.2115	1.6	3
$51\bar{4}$	0.2143	0.2141	1.5	3
711	0.2172	0.2172	3.4	5
$11\bar{5}$	0.2381	0.2379	2.0	3.5
421	0.2486	0.2489	2.4	4.5
023	0.2555	0.2562	2.1	4.5
115	0.2558		0.3	
802	0.2569		0.6	
$80\bar{4}$	0.2670	0.2662	1.1	3
006	0.2848	0.2854	0.6	3
514	0.2849		0.1	
620	0.2951	0.2947	0.5	3

Table XVIII. Continued.

hkl	$\sin^2\theta$ Calculated[a]	$\sin^2\theta$ Observed	Intensity Calculated[b]	Intensity Observed[c]
$71\bar{5}$	0.3329	0.3329	0.8	4
10,0,1	0.3333		0.5	
714	0.3729	0.3746	1.1	6
$82\bar{1}$	0.3751		1.1	
424	0.3884	0.3887	0.8	3.5
316	0.3904		0.8	
$42\bar{5}$	0.3960	0.3971	1.2	3.5
623	0.3981		0.4	
11,1,$\bar{1}$	0.4070	0.4063	1.2	3
225	0.4121	0.4127	0.3	2
$91\bar{5}$	0.4137		0.2	
822	0.4412	0.4417	0.5	3.5
330	0.4425		0.8	
12,0,0	0.4432		0.2	
$51\bar{7}$	0.4489	0.4507	0.6	3.5
12,0,$\bar{3}$	0.4508		0.3	
$82\bar{4}$	0.4514		1.0	
606	0.4592	0.4603	0.3	3
$22\bar{6}$	0.4603		0.2	
516	0.4608		0.3	
11,1,$\bar{4}$	0.4673	0.4690	0.9	4
026	0.4692		0.6	
914	0.4855	0.4869	0.3	4
$80\bar{7}$	0.4857		0.4	
10,2,$\bar{2}$	0.4884		0.3	
11,1,2	0.4890		0.9	
$33\bar{3}$	0.4978	0.4979	0.5	3
10,2,1	0.5177	0.5176	0.5	3

Table XVIII. Continued.

hkl	$\sin^2\theta$ Calculated[a]	$\sin^2\theta$ Observed	Intensity Calculated[b]	Intensity Observed[c]
333	0.5296	0.5298	0.9	3
$73\bar{2}$	0.5725	0.5718	0.8	5
731	0.5858	0.5856	0.9	5
$14,0,\bar{1}$	0.5864		0.3	
$13\bar{5}$	0.6068	0.6045	0.6	3
$82\bar{7}$	0.6701	0.6717	0.6	4
$11,1,\bar{7}$	0.6701		0.4	
427	0.6707		0.1	
717	0.6711		0.4	
$42\bar{8}$	0.6834	0.6839	0.4	3
14,0,2	0.6843		0.3	
11,1,5	0.7133	0.7154	0.4	2
136	0.7134		0.1	
$15,1,\bar{3}$	0.7303	0.7307	0.9	3.5
228	0.7313		0.3	
734	0.7416	0.7412	0.7	3.5
627	0.7570	0.7586	0.3	1.5
336	0.7591		0.6	
$11,3,\bar{1}$	0.7756	0.7751	1.0	2
$44\bar{2}$	0.8041	0.8058	1.0	3
$22\bar{9}$	0.8057		0.2	
029	0.8252	0.8241	0.2	1.5
$5,1,\overline{10}$	0.8259		0.4	
$11,3,\bar{4}$	0.8360	0.8343	1.0	1.5

Table XVIII. Continued.

hkl	$\sin^2\theta$ Calculated[a]	$\sin^2\theta$ Observed	Intensity Calculated[b]	Intensity Observed[c]
14,2,2	0.8686	0.8682	0.9	2
229	0.8693		0.4	
$53\bar{8}$	0.9274	0.9266	0.2	3 broad
$9,1,\bar{10}$	0.9276		0.3	
$84\bar{1}$	0.9281		1.3	

[a]Calculated using a = 14.124 A; b = 3.591 A; c = 8.809 A; β = 100.31 degrees with $\lambda(\bar{\alpha})$ = 1.54178 A.

[b]Calculated using the POWD intensity program assuming the atomic coordinates of Sm_2O_3. The calculation was scaled such that the most intense line had an intensity of 10.0.

[c]Estimated visually on a scale from 10 to 1.

The sesquioxides of the lanthanides are known to exhibit three different structures.[42] The low temperature stable form of all the members of the series is the body centered cubic Mn_2O_3 structure. For the elements lighter than Pm, the high temperature stable phase is the hexagonal La_2O_3 structure and for Pm through Ho, the high temperature phase is the monoclinic Sm_2O_3 structure. For the heaviest rare earths, the cubic phase is stable to the melting point. From considerations of crystallographic radii, it would be reasonable to expect the behavior of Cf^{+3} to be similar to that of Sm^{+3}. On this basis, it is not surprising that Cf_2O_3 exhibits the Sm_2O_3 structure. Further, one may note that the transitions from the cubic to monoclinic sesquioxides in the rare earths are typically slow in dry air, requiring extended annealing times to produce a crystallographically pure and reasonably well crystallized monoclinic phase even at temperatures considerably above the reported transition points.[43] During the preparation of the Cf_2O_3 samples, the temperature was as high as 1200-1250°C for approximately 5 minutes during the bead ignition and at 600°C for 1 hour during the reduction. If one assumes that a cubic to monoclinic structure change occurs in the case of Cf_2O_3 and that the kinetics of the transition are similar to those of the rare earths, it is reasonable to postulate that the transition temperature for such a structure change in Cf_2O_3 is relatively low and that the monoclinic phase was probably formed during the air ignition of the bead. Unfortunately, no x-ray data are available for the unreduced oxide; therefore, it is not possible to reach firm conclusions regarding the relative stoichiometry of the reduced and unreduced phases. It seems somewhat unlikely, however, that such a structure would exhibit a wide range of stable compositions. It is also interesting to note that the color of both reduced and unreduced Cf_2O_3 samples was a light yellow; whereas similar oxides, containing heavily mixed oxidation states, tend to be dark in color. These arguments suggest that the air ignited oxide of californium approximates the sesquioxide stoichiometry. This would be in marked contrast to the

lighter actinides which in every case form higher oxides on air ignition; in fact, the oxides of Np, Pu, Am, Cm and Bk[46] formed by air ignition approximate dioxides and all show the fluorite structure.

Because of differences in coordination and packing efficiency, the correlation of quantities derived from cell dimensions, such as molecular volumes, ionic radii, etc., should be based on calculations for the same structure type. Since californium exhibits the only monoclinic sesquioxide observed for the actinides, this is not possible in this instance. In the case of the rare earths the molecular volume for the cubic modification is considerably larger than the corresponding hexagonal or monoclinic modifications. Extrapolated molecular volumes for the hexagonal and monoclinic phases appear to be more or less comparable, the monoclinic modifications having a slightly larger volume. Whether or not the latter observation applies to the actinide sesquioxides to any high accuracy is unknown. The situation with the actinides is further complicated by the fact that the identity and lattice parameters of the observed sesquioxide modifications are possibly quite sensitive to minor variations in stoichiometry, as well as the temperature at which the system was equilibrated. Such a sensitivity has been amply demonstrated in the case of plutonium.[37] Table XIX presents the lattice parameter and molecular volume data available for the hexagonal modifications of the sesquioxides of Pu, Am, and Cm, as well as the monoclinic Cf compound. In view of the above discussion, the comparison of these data should be made with caution.

Future work on this system should certainly include crystallographic studies of the unreduced air ignited oxide and an attempt to prepare the low temperature modification of the oxide. The preparations used in this study are not appropriate for the production of a low temperature oxide. Such a preparation could be done utilizing the following set of reactions:

$$Cf^{+3}\ (\text{bead}) \xrightarrow[\text{ignite}]{\text{air}} \text{High temperature oxide}$$

Table XIX. Actinide sesquioxide lattice parameters and molecular volumes.

	a (A)	b (A)	c (A)	(deg)	Molecular volume $(A)^3$/molecule
$PuO_{1.515}$(cubic)[a]	11.04 ± 0.02				84.1 ± 0.3
Pu_2O_3(hexagonal)[a]	3.841± 0.006		5.958 ± 0.005		76.1 ± 0.2
Am_3O_3(hexagonal)[b]	3.817± 0.005		5.971 ± 0.010		75.3 ± 0.2
Cm_2O_3(hexagonal)[c]	3.80 ± 0.02		6.00 ± 0.03		74.5 ± 0.7
Cf_2O_3(monoclinic)	14.124± 0.020	3.591 ± 0.003	8.809 ± 0.013	100.31 ± 0.02	73.3 ± 0.2

[a]Reference 37.

[b]Reference 44.

[c]Reference 45.

$$\text{High temperature oxide} \xrightarrow[500^{\circ}C]{HCl} CfCl_3$$

$$CfCl_3 \xrightarrow[\Delta]{H_2O(g)} \text{Low temperature oxide}$$

2. Californium Trichloride

Diffraction data were recorded and analyzed for two $CfCl_3$ preparations. A pattern for the crystal of $CfCl_3$ was taken but could not be measured. Superposition of this film with the powder patterns demonstrated that the structures were the same and that the lattice parameters were at least very similar. The structure is the hexagonal UCl_3[47] type exhibited by the light actinides and lanthanides. The lattice parameters computed for the two powder patterns are given in Table XX. A comparison between observed and calculated $\sin^2\theta$ and intensity data is given in Table XXI.

Figure 14 is a plot of the a parameter for the UCl_3 type actinide trichlorides and Fig. 15 is a plot of the c parameter. Figure 16 is a plot of the molecular volumes of these structures. Figure 17 is a plot of the ionic radii for the actinides, computed from the lattice parameter data in Table XXII. These radii were computed from weighted averages of the nearest neighbor cation-anion distances assuming the ionic radius of the chloride ion to be 1.81 A.[51] These correlations indicate that, apparently, as the cation radius decreases, electrostatic interactions draw the six apical chloride ions closer to the cation, thus shrinking the c axis. As this occurs, however, repulsive interactions between the apical chlorides and particularly between the apical chlorides and the equitorial chlorides tend to prevent a similar shrinkage in the length of the a axis. This anion crowding becomes so severe, that the shrinkage of the a axis with increasing atomic number is sharply curtailed after plutonium. In view of the californium results, it would appear, in fact, that the a parameter begins to expand slightly with increasing atomic number after curium, even though the molecular volume and ionic radius continue to decrease.

Table XX. Californium trichloride lattice parameters-hexagonal UCl_3 structure.

Film number	a (A)	$2\sigma a$[a] (A)	c (A)	$2\sigma c$[a] (A)
2368 A	7.390	0.003	4.095	0.003
2430 A	7.396	0.002	4.085	0.002
Average[b]	7.393	0.040	4.090	0.060

[a]Estimated standard deviation as computed from least squares fits using the LCR-2 lattice parameter program.

[b]The error limits placed on the average values were computed using

$$95\% \text{ confidence error limit} = \frac{12.71}{\sqrt{N}} \sqrt{\frac{\Sigma d_i^2}{N-1}}$$

where d_i is the deviation of the individual lattice parameters from the average; N is the number of observations, i.e., 2; and the factor 12.71 is the 95% confidence student t value for 2 observations.

Table XXI. Line list and indexing for hexagonal californium trichloride - Film 2430 A

hkl	$\sin^2\theta$		Intensity	
	Calculated[a]	Observed	Calculated[b]	Observed[c]
101	0.0500	0.0501	10.0	10
200	0.0580	0.0580	2.4	7
111	0.0790	0.0788	1.0	4.5
201	0.0935	0.0932	9.2	10
210	0.1015	0.1010	1.5	5
300	0.1305	0.1302	3.6	8.5
121	0.1370	0.1373	7.7	10
002	0.1421	0.1425	1.5	5
102	0.1566	0.1575	1.0	5
220	0.1740	0.1736	1.4	5.5
112	0.1856	0.1860	2.1	8
202	0.2001	0.2001	0.8	4.5
131	0.2240	0.2236	2.4	8
400	0.2320	0.2306	0.4	3
212	0.2436	0.2435	0.8	4.5
401	0.2675	0.2663	0.7	2
302	0.2726	0.2730	2.2	8
140	0.3044	0.3038	1.3	4.5
231	0.3110	0.3106	2.8	7.5
222	0.3161	0.3166	1.1	4
312	0.3306	0.3297	0.5	3.5
103	0.3342	0.3354	0.7	3.5

Table XXI. Continued.

hkl	$\sin^2\theta$		Intensity	
	Calculated[a]	Observed	Calculated[b]	Observed[c]
500	0.3624	0.3637	0.2	2
113	0.3632		0.1	
203	0.3777	0.3789	1.0	4
501	0.3980	0.3984	1.0	3.5
213	0.4212	0.4230	1.3	6
241	0.4414	0.4406	1.1	3
142	0.4465	0.4481	1.5	5
151	0.4849	0.4845	1.2	5
133	0.5082	0.5089	0.7	4
332	0.5335	0.5338	0.6	4
341	0.5719	0.5706	0.8	3
233	0.5952	0.5961	1.2	5
161	0.6589	0.6570	0.8	3
602	0.6640	0.6628	0.5	3
503	0.6822	0.6821	0.7	3
304	0.6989	0.6995	0.8	3
252	0.7075	0.7078	1.4	3
243	0.7256	0.7264	0.9	3
701	0.7459	0.7456	0.4	3.5
351			1.0	
153	0.7691	0.7706	1.2	3.5
261	0.7894	0.7894	1.0	2.5
170	0.8263	0.8247	1.0	2

Table XXI. Continued

hkl	$\sin^2\theta$ Calculated[a]	$\sin^2\theta$ Observed	Intensity Calculated[b]	Intensity Observed[c]
442	0.8380	0.8388	0.9	2.5
343	0.8561	0.8564	1.1	3
144	0.8728	0.8739	1.8	3.5 broad
163	0.9431	0.9429	1.2	2.5 broad
172	0.9684	0.9687	4.4	2.5 broad

[a] Calculated using $a = 7.393$ A and $b = 4.090$ A with $\lambda = 1.54178$ A.

[b] Calculated using the POWD intensity program assuming the atomic coordinates of UCl_3. The calculation was scaled such that the strongest line had an intensity of 10.0.

[c] Estimated visually on a scale from 10 to 1.

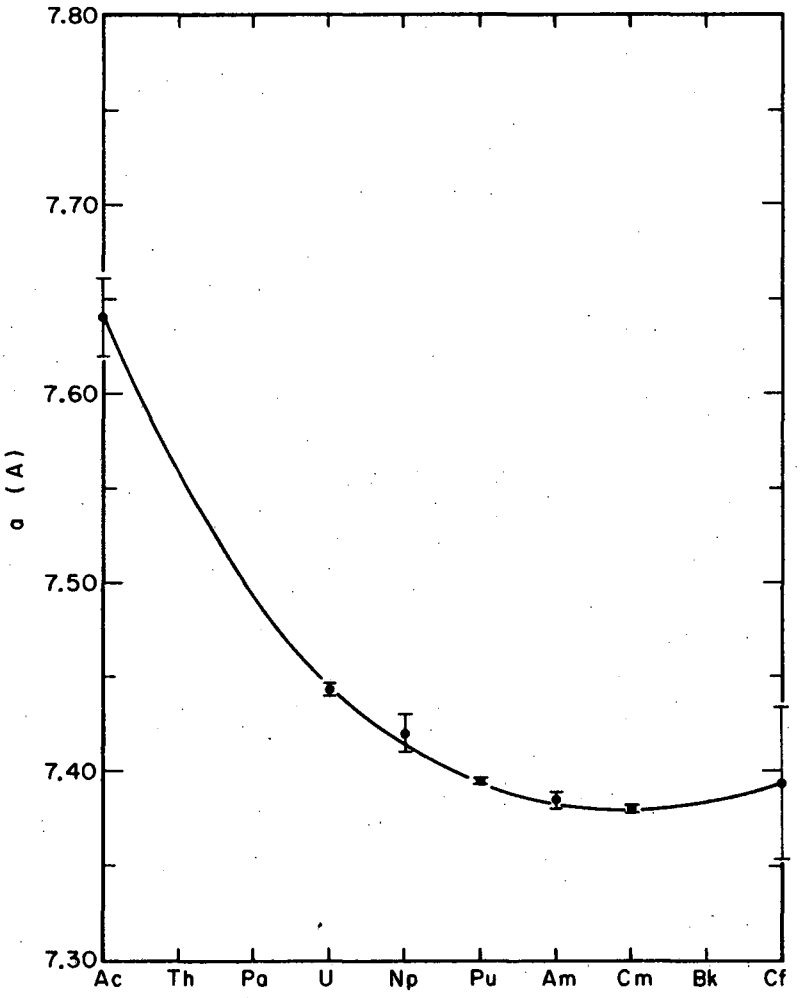

Fig. 14. Comparison of the a parameters for the UCl_3 type actinide trichlorides.

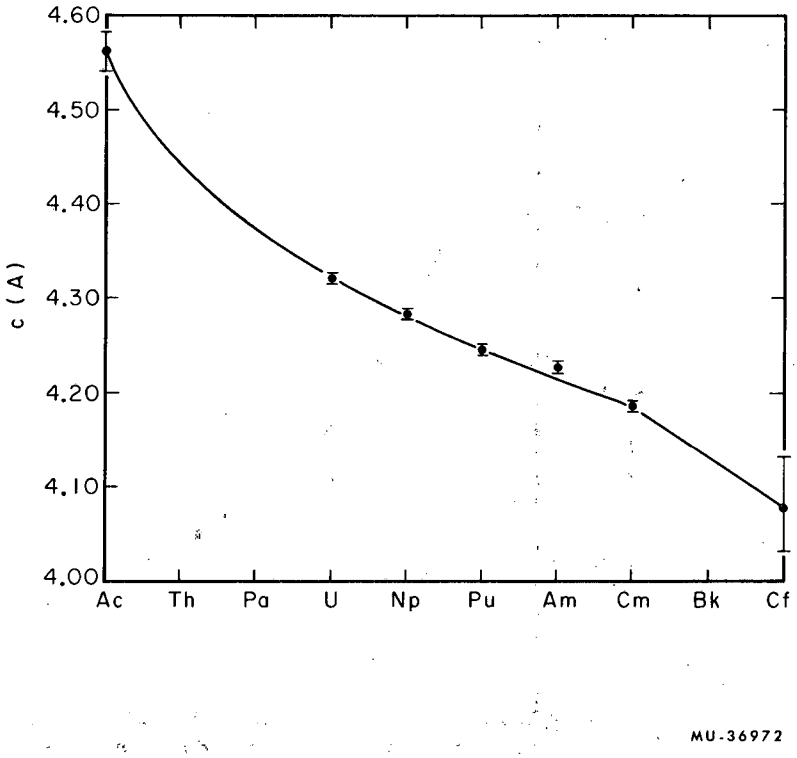

Fig. 15. Comparison of the c parameters for the UCl_3 type actinide trichlorides.

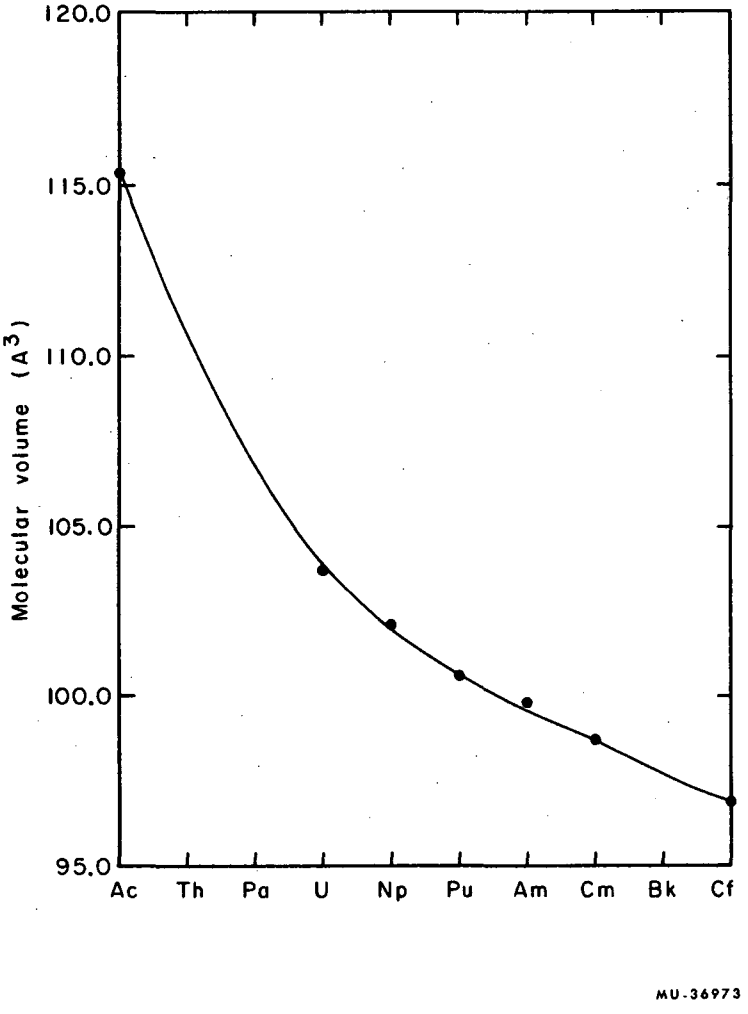

Fig. 16. Comparison of the molecular volumes of the UCl_3 type actinide trichlorides.

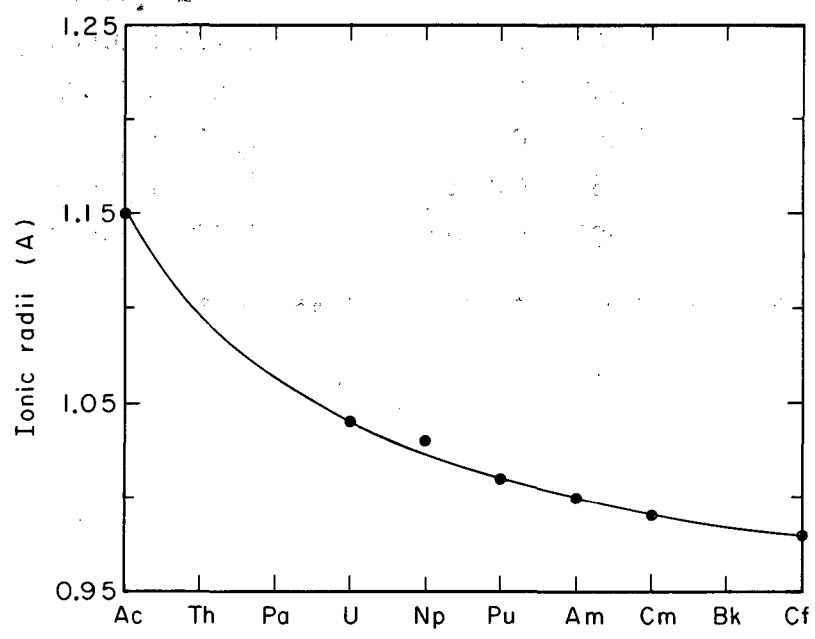

Fig. 17. Crystallographic radii for the tripositive actinides as calculated from trichloride data. (Corrected to a coordination number of 6.)

Table XXII. Actinide trichloride lattice parameter data.

	a (A)	c (A)	Reference
Ac	7.64 ± 0.02	4.56 ± 0.02	48
U	7.443 ± 0.003	4.321 ± 0.003	48
Np	7.420 ± 0.010	4.282 ± 0.005	48
Pu	7.395 ± 0.001	4.246 ± 0.001	48
Am	7.384 ± 0.004	4.225 ± 0.004	49
Cm	7.380 ± 0.001	4.185 ± 0.001	50
Cf	7.393 ± 0.040	4.090 ± 0.060	-

In the lanthanide series, the trichlorides of La through Gd exhibit the UCl_3 structure.[52] In the case of $TbCl_3$, the orthorhombic $PuBr_3$ structure has become the stable modification.[53] If it may be assumed that the radius ratio controls the crystallographic configuration of these materials, the $PuBr_3$ structure would not be expected for the actinide trichlorides until quite late in the series.

V. SUMMARY

Californium has recently become available in quantities sufficient to allow studies to be initiated on its bulk chemical and physical properties. The material available for the present study was 6 μg of Cf^{249} which was derived from the decay of Bk^{249}. This amount of material was adequate for the proposed studies; however, several major problems are associated with procedures applicable to purifications on this scale. Even using microtechniques, wet chemical operations involve rather dilute solutions, e.g., 10^{-5} to 10^{-4} M in californium. This results in marked sensitivity to recontamination during processing, particularly with respect to cations with low atomic weight. Such "background" contamination was avoided as much as possible by first minimizing the availability of contaminants, i.e., operating in very clean systems and using very pure reagents and second by maximizing the concentration of the californium by volumetrically scaling down the operations. Except for changes necessitated by these problems, the purification operations were essentially those which have become standard in actinide chemistry.

Due to the considerable difficulties involved in the purification techniques, it was considered essential that analytical procedures be developed to evaluate the purity of the preparations prior to their use. Using mass analysis techniques, the Nd content was determined to be 0.32 atom %, and total rare earths were estimated at approximately 1.6 atom %. Using alpha pulse height analysis, Cm^{244} was estimated at < 1 atom %, Am < 1 atom % and although it is not possible to set a quantitative limit for Pu, it is felt that chemical and spectroscopic evidence indicated its absence. The single bead assay technique indicated that other materials are potentially present as contaminants. Chemical and relative abundance arguments lead to the tentative identification of the most probable contaminants as Al and Ca.

Absorption spectrum data was recorded for Cf^{+3} absorbed on beads of cation exchange resin and as hydrated californium chloride. It is suggested that these data should closely approximate the solution spectrum of Cf^{+3}. By comparison of the Cf^{+3} bead spectra with the spectrum of Pr^{+3} taken under identical conditions, the molar extinction coefficients of Cf^{+3} in solution were estimated to be between 1 and 10 for the transitions observed. Room temperature absorption data were also recorded using a crystal of $CfCl_3$. Preliminary calculations were carried out by Dr. K. Rajnak fitting these data to a theoretical energy level scheme. The least squares fits obtained appear to be satisfactory; however, it will not be possible to be certain about J-level assignments until low temperature data are available. This should clearly be an early objective for future studies.

Samples of Cf_2O_3 were prepared and characterized crystallographically using x-ray powder techniques. This compound was found to exhibit the monoclinic Sm_2O_3 structure with $a = 14.124 \pm 0.020$ A, $b = 3.591 \pm 0.003$ A, $c = 8.809 \pm 0.013$ A, and $\beta = 100.31 \pm 0.02$ deg. It is suggested that this structure crystallized during the final stages of the air ignition of the bead. This implies that the air ignited oxide of californium approximates the sesquioxide stoichiometry. This is in direct contrast to the behavior of the lighter actinides which form higher oxides under similar treatment. Samples of $CfCl_3$ were also prepared and characterized. This compound was found to exhibit the hexagonal UCl_3 structure with $a = 7.393 \pm 0.040$ A and $c = 4.090 \pm 0.060$ A. The ionic radius for Cf^{+3} computed from the chloride data is 0.98 A. This indicates an actinide contraction of 0.01 A between Cm^{+3} and Cf^{+3}.

ACKNOWLEDGMENTS

It is with pleasure that I express my sincere thanks to Professor Burris B. Cunningham. Our discussions and his many suggestions were often instrumental in the solution of the problems at hand, while his personal interest and infectious enthusiasm were of constant encouragement. His thoughtful guidance made my work here an educational experience unequaled in my career.

I would also like to take this opportunity to express my thanks to the late Dr. James C. Wallmann. It was largely through Jim that I was introduced to the fascinating techniques involved in this study. I will always consider the time spent under his tutelage to be of primary importance to my professional development.

Special notes of thanks must go to Dr. Katheryn Rajnak for her analysis of the spectroscopic data, to Mr. Joseph R. Peterson for his careful assistance during many phases of the work, to Mr. Ralph D. McLaughlin whose patient advice and expert assistance were of extreme value during the spectroscopic studies, and to Mr. R. D. Baybarz of ORNL, who provided very valuable assistance during the purification of the first californium preparation and during the early single bead spectroscopic studies. I would also like to thank Dr. Maynard Michel for running the mass analyses and for many helpful suggestions regarding high purity operations and to thank Mr. Tom Parsons for his help and many suggestions.

The laboratory assistance of Miss Lilly Goda and Mrs. Lillian White is greatly appreciated as are the efforts of the Health Chemistry Division in general and Mrs. Gertrude Bolz in particular.

My greatest debt, however, is to my wife whose moral support kept my spirits high and whose understanding and patience made my work possible.

This work was performed under the auspices of the United States Atomic Energy Commission.

REFERENCES

1. G. T. Seaborg and A. R. Fritsch, Sci. Amer. 208, 68 (1963).
2. B. B. Cunningham, Microchemical Journal, Symposium (1961).
3. B. B. Cunningham, Proceedings of the Robert A. Welch Foundation Conferences on Chemical Research, VI. Topics in Modern Inorganic Chemistry, 1962.
4. D. F. Peppard, S. W. Moline, and G. W. Mason, J. Inorg. Nucl. Chem. 4, 344 (1957).
5. R. C. Petterson, Lawrence Radiation Laboratory Report, UCRL-11074 (1963).
6. D. B. McWann, B. B. Cunningham, and J. C. Wallmann, J. Inorg. Nucl. Chem. 24, 1025 (1962).
7. G. H. Higgins, Lawrence Radiation Laboratory Report, UCRL-6134 (1960).
8. J. P. Surls, Jr., Lawrence Radiation Laboratory Report, UCRL-3209 (1956).
9. R. M. Diamond, K. Street, Jr., and G. T. Seaborg, J. Am. Chem. Soc. 76, 1461 (1954).
10. K. Street, Jr. and G. T. Seaborg, J. Am. Chem. Soc. 72, 2790 (1950).
11. G. R. Choppin, B. G. Harvey, and S. G. Thompson, J. Inorg. Nucl. Chem. 2, 66 (1956).
12. R. J. Walker and T. R. Corbin, Lawrence Radiation Laboratory Report, UCRL-16467 (1965).
13. R. M. Latimer, Lawrence Radiation Laboratory, private communication (1965).
14. M. G. Inghram, Ann. Rev. Nuc. Sc. 4, 81 (1954).
15. R. C. Vickery, Chemistry of the Lanthanons, (Academic Press Inc., New York, 1953), p. 16.
16. D. Strominger, J. M. Hollander, and G. T. Seaborg, Rev. Mod. Phys. 30, 585 (1958).
17. J. Milsted, Argonne National Laboratory, private communication (1965).
18. D. Metta, H. Diamond, R. F. Barnes, J. Milsted, J. Gray, Jr., D. J. Henderson, and C. M. Stevens, J. Inorg. Nucl. Chem. 27, 33 (1965).

19. N. H. Nachtrieb, Principles and Practice of Spectrochemical Analysis (McGraw-Hill Book, Co., Inc., New York, 1950).
20. F. W. E. Strelow, Anal. Chem. 32, 1185 (1960).
21. D. C. Stewart, Lawrence Radiation Laboratory Report, AECD-2389 (1948).
22. W. T. Anderson, Jr., Op. Soc. Amer. 41, 385 (1951).
23. Eastman Kodak Co., Kodak Photographic Plates for Scientific and Technical Use (1953).
24. E. H. Carlson and G. H. Dieke, J. Chem. Phys. 34, 1602 (1961).
25. K. Rajnak, Lawrence Radiation Laboratory, unpublished calculations for Cf^{+3}.
26. K. Rajnak, J. Opt. Soc. Amer. 55, 126 (1965).
27. K. Rajnak, J. Chem. Phys. 43, 847 (1965).
28. B. G. Wybourne, Spectroscopic Properties of Rare Earths, (Interscience Publishers, New York, 1965).
29. K. Rajnak and B. G. Wybourne, Phys. Rev. 132, 280 (1963).
30. J. Conway and K. Rajnak, Lawrence Radiation Laboratory, unpublished calculations for U^{+3}.
31. K. Rajnak, Argonne National Laboratory, and W. F. Krupke, Dept. of Physics, UCLA, unpublished calculations for Np^{+3}.
32. J. Conway and K. Rajnak, J. Chem. Phys. (January 1966), to be published.
33. P. R. Fields, B. G. Wybourne, and W. T. Carnall, Argonne National Laboratory Report, ANL-6911 (1964).
34. J. G. Conway, J. B. Gruber, E. K. Hulet, R. J. Morrow, and R. G. Gutmacher, J. Chem. Phys. 36, 189 (1962).
35. B. B. Cunningham, Lawrence Radiation Laboratory, private communication (1963).
36. L. B. Asprey, Ph. D. Thesis, University of California, Lawrence Radiation Laboratory Report, UCRL-329 (1949).
37. E. R. Gardner, T. L. Markin, and R. S. Street, J. Inorg. Nucl. Chem. 27, 541 (1965).

38. D. K. Smith, Lawrence Radiation Laboratory Report, UCRL-7196 (1963).
39. D. E. Williams, Ames Laboratory Report, IS-1052 (1964).
40. D. T. Cromer, J. Phys. Chem. 61, 753 (1957).
41. F. Weigel, Institut für Anorganische Chemie der Universität München, Munich, West Germany, private communication (1965).
42. L. Eyring and B. Holmberg, Chapter 4, Nonstoichiometric Compounds, edited by R. E. Gould, Amer. Chem. Soc. (1963).
43. I. Warshaw and R. Roy, J. Phys. Chem. 65, 2048 (1961).
44. D. H. Templeton and C. H. Dauben, J. Am. Chem. Soc. 75, 4560 (1953).
45. J. C. Wallman, J. Inorg. Nucl. Chem. 26, 2053 (1964).
46. B. B. Cunningham, Lawrence Radiation Laboratory and J. C. Wallman (deceased), private communication (1963).
47. W. H. Zachariasen, Paper 20.6, National Nuclear Energy Series, Vol. IV - 14B (1949).
48. W. H. Zachariasen, Chapter 18, National Nuclear Energy Series, Vol. IV - 14A (1949).
49. J. Fuger, to be submitted to J. Inorg. Nucl. Chem.
50. J. C. Wallmann, J. Fuger, J. R. Peterson, and J. L. Green, to be published in J. Inorg. Nucl. Chem.
51. L. Pauling, The Nature of the Chemical Bond (Cornell University Press, Ithaca, New York, 1948).
52. W. H. Zachariasen, Acta Cryst. 1, 265 (1948).
53. J. D. Forrester, A. Zalkin, D. H. Templeton, and J. C. Wallmann, Inorg. Chem. 3, 185 (1964).
54. G. H. Brown and E. M. Sollee, Quantitative Chemistry (Prentice-Hall, Inc., Englewood Cliffs, N. J., 1963).